CANADIAN THESES ON MICROFICHE

THÈSES CANADIENNES SUR MICROFICHE

National Library of Canada
Collections Development Branch

Canadian Theses on
Microfiche Service

Ottawa, Canada
K1A 0N4

Bibliothèque nationale du Canada
Direction du développement des collections

Service des thèses canadiennes
sur microfiche

NOTICE

The quality of this microfiche is heavily dependent upon the quality of the original thesis submitted for microfilming. Every effort has been made to ensure the highest quality of reproduction possible.

If pages are missing, contact the university which granted the degree.

Some pages may have indistinct print especially if the original pages were typed with a poor typewriter ribbon or if the university sent us an inferior photocopy.

Previously copyrighted materials (journal articles, published tests, etc.) are not filmed.

Reproduction in full or in part of this film is governed by the Canadian Copyright Act, R.S.C. 1970, c. C-30. Please read the authorization forms which accompany this thesis.

AVIS

La qualité de cette microfiche dépend grandement de la qualité de la thèse soumise au microfilmage. Nous avons tout fait pour assurer une qualité supérieure de reproduction.

S'il manque des pages, veuillez communiquer avec l'université qui a conféré le grade.

La qualité d'impression de certaines pages peut laisser à désirer, surtout si les pages originales ont été dactylographiées à l'aide d'un ruban usé ou si l'université nous a fait parvenir une photocopie de qualité inférieure.

Les documents qui font déjà l'objet d'un droit d'auteur (articles de revue, examens publiés, etc.) ne sont pas microfilmés.

La reproduction, même partielle, de ce microfilm est soumise à la Loi canadienne sur le droit d'auteur, SRC 1970, c. C-30. Veuillez prendre connaissance des formules d'autorisation qui accompagnent cette thèse.

THIS DISSERTATION
HAS BEEN MICROFILMED
EXACTLY AS RECEIVED

LA THÈSE A ÉTÉ
MICROFILMÉE TELLE QUE
NOUS L'AVONS REÇUE

Canada

NL 339 (r. 86/09)

A Microprocessor System for the Characterisation of Arterial Pulse Waves Obtained from Microwave Impedance Measurements

by

Alain A. Menard

A thesis
presented to University of Ottawa
in partial fulfillment of the
requirements for the degree of
M.A.Sc.
in
Department of Electrical Engineering

UNIVERSITÉ D'OTTAWA
UNIVERSITY OF OTTAWA

ABSTRACT

In this thesis, a microprocessor system for the characterisation of arterial pulse waves obtained from microwave impedance measurements is described. The microwave pulse recorder, or MPR, makes use of a Doppler radar at microwave frequencies, to obtain signals proportional to the time varying impedance of biological tissues as blood vessels pulsate. The main objective of this thesis was to design a system capable of extracting useful information from these signals, namely the pulse wave velocity and the pulse transit times along arterial segments in humans. Physiological principles involved in arterial circulation are first presented, then followed by a review of existing techniques for arterial pulse wave acquisition and analysis. A discussion of the signal processing theory involved with information extraction aspects is then presented. This is followed by a description of the design of a simulation system implemented to determine system design parameters as well as to develop information extraction algorithms. Finally, experimental results are presented together with a discussion of the system design performance, advantages, and shortcomings.

ACKOWLEDGEMENTS

The author wishes to express his gratitude to his supervisor, Professor M. Goldberg, for his guidance throughout the course of this research.

Thanks are also due to other members of the Department of Electrical Engineering, especially Dr. A. Smith, Mohammed Master and Steve Symmons for their invaluable assistance in the execution of this project.

LIST OF FIGURES

LIST OF SYMBOLS

ADC	Analog-to-digital converter
α	The attenuation of microwaves in water
b_n	The coefficients of a non-recursive filter
bpi	Density of magnetic tape in bits per inch
c(t)	The autocovariance of a sampled function
CCD	Charged couple device
CPU	Central processing unit
CSR	The cardiovascular signal recorder system
d(i)	The least squares estimate of the first derivative of a function
DMAC	Direct memory access controller
$\triangle P$	The pressure difference between two ends of a tube
$\triangle PM$	The peak detection algorithm uncertainty
$\triangle QTM$	The uncertainty due to quantization error in MPR signal
$\triangle QTR$	The uncertainty due to quantization error in ECG signal
$\triangle RW$	The R-wave detection algorithm uncertainty
$\triangle STM$	The uncertainty due to finit sampling rate in MPR signal
$\triangle STR$	The uncertainty due to finit sampling rate in ECG signal
$\triangle TRP$	The R-wave to peak MPR time uncertainty
E	Young's modulus of elasticity in a tube
E_p	The pressure elastic modulus
e(t)	The interpolator mean squared error function
ECG	The electrocardiogram

F	The flow rate in a tube
$f_s(t), f$	A sampled function
$f_r(t)$	The reconstruted function from a sampled function
$F_s(\omega)$	The Fourier transform of a sampled function
$F_r(\omega)$	The Fourier transform of a reconstructed function
f_s	The sampling frequency
q_m	The values of a filtered function
γ	The ratio of arterial wall thickness to wall radius
h	The thickness of an arterial wall
$H_N(j\omega)$	The approximate transfer function of a non-recursive filter
$H_d(j\omega)$	The desired transfer function of a non-recursive filter
$I(\omega)$	The interpolating function
IOP	Input Output processor
ips	The speed of a tape drive in inches per second
L	The lenght of a tube
λ	The wavelength of microwaves in water
MMU	Memory management unit
MPR	The microwave pulse recorder
η	The viscosity of a fluid
n	The number of bits per quantization word
ω_o	The frequency of MPR transmitter signal
PIC	Programmable interrupt controller
PIO	Programmable input output controller
PIT	Programmable interval timer

PTT	The pulse transit time from ECG R-wave to peak arterial pulse
PWV	The pulse wave velocity in an artery
R	The internal radius of an arterial vessel
ρ	The density of blood
S	The quantization step size
SHA	A sample and hold amplifier
SNR	The signal to noise ratio
T	The sampling time interval
Θ_T, Θ_R	The phase of MPR transmitter and receiver signals
TMP	Arterial transmural pressure
V_T, V_R	The amplitude of MPR transmitter and receiver signals
w(t)	The data window function
$Z_{AA}(t)$	A template digitized arterial pulse signal

CONTENTS

Chapter I

INTRODUCTION

Occlusions in the arterial system is one of the major cause of mortality in man. Evaluation of the location and extent of arterial related disease are necessary pre-operative steps. Several studies have demonstrated that useful diagnostic information may be derived from the characterization of the arterial pulse pressure wave.

Traditional techniques for obtaining the pulse pressure waves in arteries are invasive in nature, involving the insertion of special pressure transducers in the patient's artery, and therefore incurs certain risks. This limits the usefulness of pulse characterization techniques to situations where the condition of the patient justifies the use of invasive transducers and the potential for inherent complications.

More recently, ultrasound transducers have been used to obtain arterial pulse pressure signals non-invasively. Even though ultrasound techniques have proven successful, their usefulness is limited to the evaluation of pulses from

peripheral arteries because of their low penetration depth in human tissues, particularly in bone and in air.

Stuchly et al., [1] proposed a microwave device for the detection of arterial wall motion, called the microwave pulse recorder (MPR). The advantage of using this device for arterial pulse wave acquisition lies in the high penetration depth, in human tissue, of signals at microwave frequencies. This gives the advantage of being able to monitor, non-invasively, the pulse wave of deeper situated arteries such as the aorta and iliac arteries. One parameter of particular interest is the arterial pulse wave velocity (PWV) at different locations in the arterial system. Several studies have correlated the variability of the PWV with changes in the mechanical properties of the arterial walls, which in turn is a function of the health of arteries.

This thesis deals with acquisition, processing, and information extraction aspects related to pulse pressure wave signals obtained from the microwave pulse recorder. For this purpose, a microprocessor based system, called the Cardiovascular signal recorder (CSR), was designed. The CSR was designed primarily for studying the usefulness of the MPR as a tool for evaluating diseases of the arterial system as characterized in pulse wave signals. Prior to the CSR design

and implementation, it was found necessary to implement a simulation system, using a microcomputer development system. With this system it was possible to determine several system design parameters and to develop processing and information extraction algorithms best suited for analysis of signals derived from the microwave pulse recorder. The following sections outline the work that comprise this thesis.

In chapter two, physiological aspects of the arterial pulse wave are discussed. The mechanics involved in blood circulation through the arterial system and a review of arterial blood flow models are presented. The clinical significance of some parameters related to the pulse pressure wave are also examined. In chapter three, some of the currently used transducers are reviewed giving particular attention to the electrocardiograph and the microwave pulse recorder.

In chapter four several aspects of digital signal processing, particularly relevant to our needs, are discussed. In chapter five digital hardware available to perform the signal processing functions are examined. In particular, a technical discussion of microprocessor systems and supporting hardware for medical applications is presented.

In chapter six, the development of the Cardiovascular signal recorder simulation system is presented. Some important system design parameters are deduced from an uncertainty analysis and real results are examined and compared with expected system performance. In chapter seven the general design of the Cardiovascular signal recorder is then given. A final discussion of results and system design capabilities and failures follows in chapter eight.

Chapter II

PHYSIOLOGY OF THE ARTERIAL PULSE WAVE

2.1 MECHANICS OF CIRCULATION

In this section we will briefly describe the mechanical events involved in the circulation of blood in the arterial system. All muscle contractions are activated by bio-electric currents. Such currents are also responsible for the contractions of the heart muscles. The electrocardiogram (ECG) is a record of the electrical activity of the heart. A typical ECG is shown in Figure 2.1(a). The P wave is caused by contraction of the atria. During this time the heart muscle is electrically polarized and then depolarized. The QRS complex is produced by ventricular depolarization and the ST segment and the T wave by ventricular repolarization.

Blood flows through the vessels primarily because of the forward motion conveyed to it by the pumping action of the heart. Contractions of the heart causes the blood in the ventricles to be forced into the aorta which in turn moves the blood forward in the arterial system, and also generates a pressure wave that expands the wall of the arteries as it travels down the arterial tree [2]. The pressure waves in

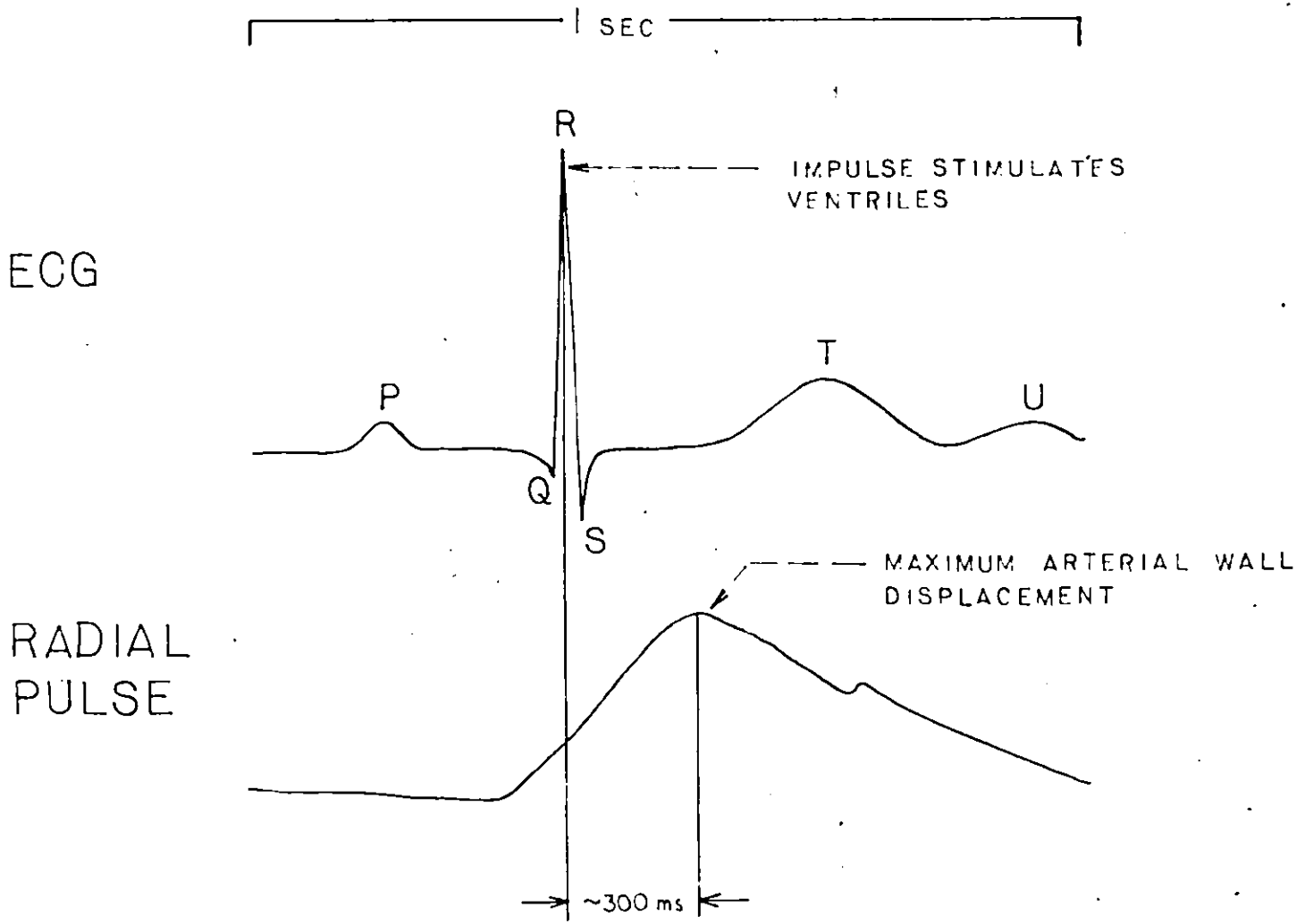

Figure 2.1 Typical ECG and Pulse Pressure Wave in radial artery of human wrist.

different arteries are shown in Figure 2.1(b). The speed at which the pressure wave travels is independant and faster than the velocity of blood flow. The pulse wave velocity (PWV) is usually in the range of 5 to 8m/s, [3]. It varies with many factors such as age, health and distance from the heart. These factors and others will be discussed in the following section.

2.2 MODELS OF THE ARTERIAL SYSTEM

The relationship between mean blood flow, mean pressure and total hydraulic resistance in the arterial system is very similar to the relationship between the voltage, current and resistance in an electrical circuit:

$$\text{FLOW} = \text{PRESSURE} / \text{RESISTANCE} \qquad (2.1)$$

The Poiseuille-Hagen equation describing the relationship between flow, viscosity and radius in a long narrow tube provides insight into the physical principle involved in blood flow;

$$F = \Delta P \pi R^4 / 8 \eta L \qquad (2.2)$$

where F is the flow rate, ΔP is the pressure difference between the two ends of the tube, R is the radius, L is the length and η is the viscosity of the fluid.

The elastic behaviour of the blood vessels is usually given in terms of wave speed as a function of the distance from the heart and the blood pressure. The PWV in an infinitely thin walled elastic vessel may be predicted from its viscoelastic properties using the so-called Moens-Korteweg equation [4]:

$$PWV^2 = Eh/2R\rho \qquad (2.3)$$

where E is the circumferential Young's modulus of elasticity h the wall thickness, R the internal vessel radius and ρ the density of the blood. For thicker walled vessels (2.3) is commonly rewritten as

$$PWV^2 = Ep(1-\gamma)/2\rho \qquad (2.4)$$

where γ is the ratio of wall thickness to external vessel radius and Ep is the pressure elastic modulus defined as

$$Ep = \Delta P\ R/\Delta R \qquad (2.5)$$

where ΔR is the change in external radius of the vessel associated with a pressure change ΔP and R is the mean vessel radius.

The validity of the Moens Korteweg equation has not been fully verified in vivo. One the problems with this equation is that it does not account for wave reflections. Wave are reflected primarily because of changes in hydraulic impedances such as the end of peripheral arteries or obstructed arteries. It is quite difficult to assess quantitatively the effect of reflections. One of the major repercussion of wave reflections is that they contribute to changing the shape of the pulse wave as it travels [5]. This makes it difficult to define a reference point on the wave when measuring its velocity. Wave reflections also cause variations in PWV. For example Westeroff [6] reported increases in PWV in a model of an obstructed artery. Another related problem stems from the non-linear elastic behaviour of the arterial wall. Wetterer [7] reported pressure-diameter diagrams showing hysteresis effect in which pressure leads diameter in canine carotid artery (Figure 2.2).

Other parameters not considered in the Moens Korteweg equation are: mechanical properties of the arterial walls, the anatomic structure of the arterial system, the type of

flow (for example artery stenosis can cause turbulent flow), and the vasoactive state of the arteries (eg. caused by drugs, hormones, etc...). Many complex models have been developed which include some of the parameters discussed, [8,9,10]. It is beyond the scope of this thesis to review this work.

2.3 CLINICAL SIGNIFICANCE OF PWV

The study of the mechanics of the arteries is important since it is related to the functions of the arteries in the circulation. For example, arterial properties influence the work of the heart since the hydraulic impedance presented to the heart by the arterial system constitutes the load of the heart. The resistance to flow depends on several factors including the viscosity of the blood and the diameter of the vessels.

Much work has been done to investigate the correlation of the PWV with other hemodynamic variables. Initially PWV was thought to be a function of mean pressure only. Gribbin et al. [11,12] showed that the coefficients of correlation relating the PWV and the brachial artery transmural pressure (TMP) in human subjects were 0.9 or greater and increased linearly with TMP, (Figure 2.3). Their study also showed no

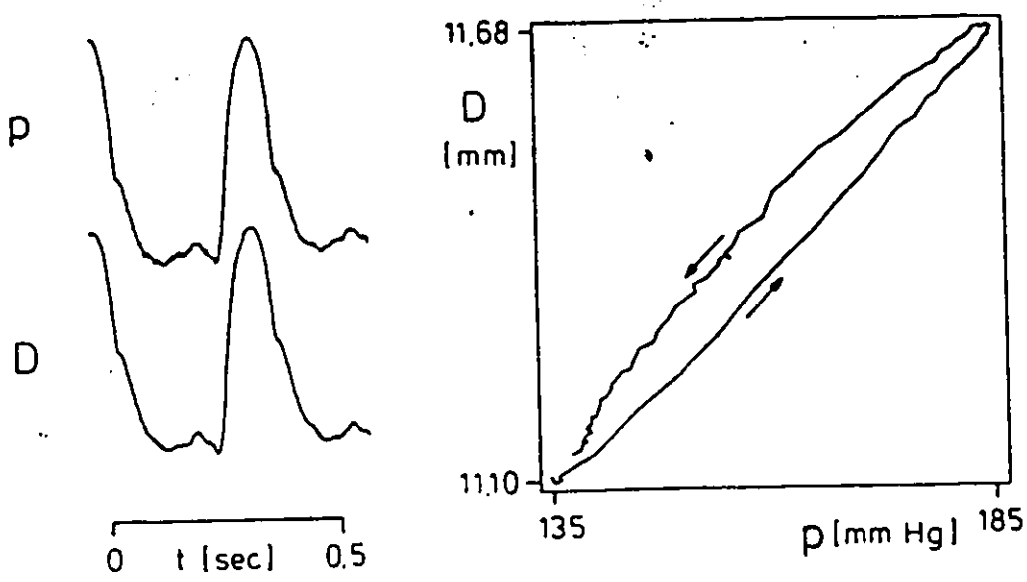

Figure 2.2 Left:time course of pressure (P) and diameter (D) in canine abdominal aorta.
Right:pressure diameter loop of pulse (from Wetterer).

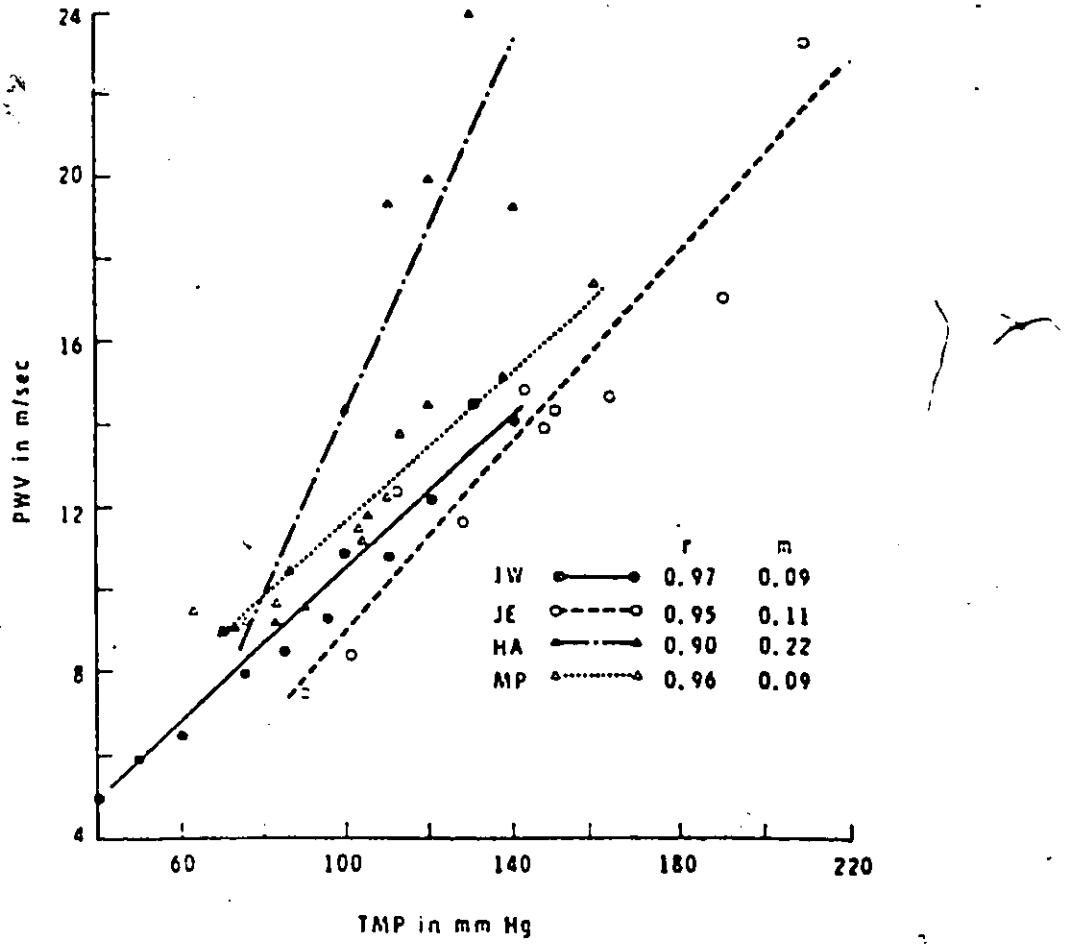

Figure 2.3 PWV plotted against TMP for 4 subjects;r is the correlation coefficient and m is the slope (from Gribbin).

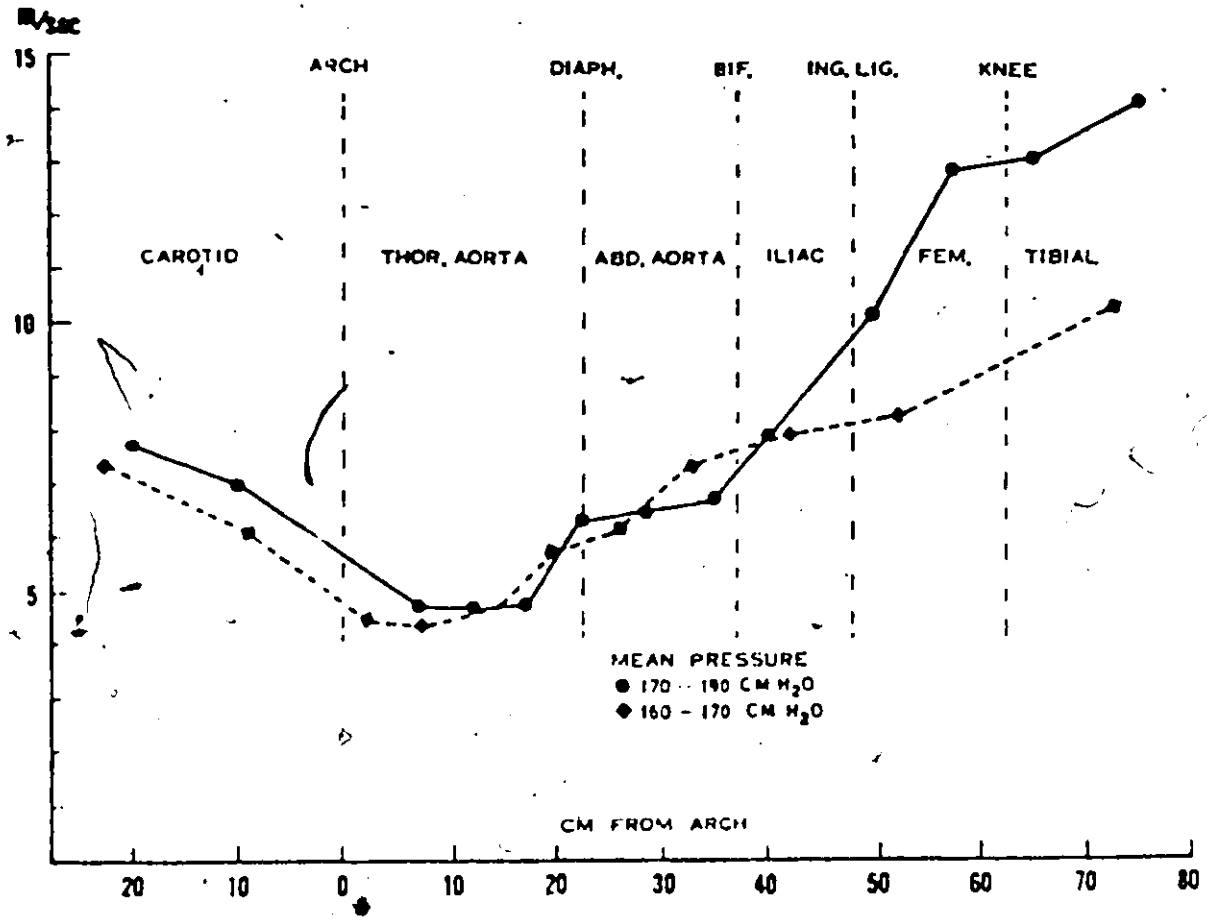

Figure 2.4 PWV plotted against anatomical position and distance from heart (from McDonald).

evidence of decline in the validity of the correlations with increasing age and resting pressure. However, slopes of the relationship (regression coefficients) varied from 0.04 to 0.25. This implies that for any one individual an absolute change in arterial pressure cannot be deduced from change in PWV alone.

Studies have shown the variability of PWV with other anatomical and physiological variables. Most of these variations were shown to be related to changes of mechanical properties of the arterial wall, [13]. This was found true not only for small vessels but also large arteries such as the aorta; for example, when vasoactive agents were present in the blood. The changes were, however, quite small in larger arteries. McDonald, [14], showed the dependance of PWV on the anatomical position and distance from the heart in dogs, (Figure 2.4). He explains that there is less variability in PWV in larger arteries because the effect of the vascular smooth muscle is greater than in smaller arteries. Other investigators reported correlation of PWV with endocrine disorders [15], and cardiovascular diseases [16].

Use of the PWV as a measure of arterial blood pressure change requires measurement of the interval between pulse arrivals at two sites along an artery segment. It is

difficult to obtain continuous trains of artefact free pulses from two sites. Also, the intervals between pulse arrivals is very short, making it difficult to measure PWV accurately. These problems can be overcome by measuring an alternate interval called the pulse transit time (PTT). The PTT is the interval from the occurence of the ECG's R-wave and the pulse transit time at a site on an artery. The PTT however, includes not only the pulse transmission time, but also the delay due to intra-cardiac events such as electrical depolarization, isovolumic contraction, the opening of semilunar valves, and expulsion of blood. Nevertheless, Gribbin et al., [11], showed a correlation between PTT and mean arterial pressure in the range of 0.91 and 0.98.

Models such as the Moens Korteweg equation and reported experimental results clearly show that PWV not only correlates with blood pressure but is also a function of the health of the arteries. This constitutes the basic rationale for this thesis.

Chapter III

PHYSIOLOGICAL TRANSDUCERS

3.1 GENERAL TRANSDUCERS

In this section we will briefly describe some of the most common transducers used in a number of medical instruments. Figure 3.1 shows some physiological parameters along with the principal measurements and frequency ranges associated with each. These ranges specify the sensitivity, dynamic range and bandwidth of the transducers.

A transducer is a device that converts energy from one form to another. Ideally transducers should only respond to the form of energy present in the physical quantity to be measured. However, there usually are interfering inputs affecting the instruments as a consequence of the principle used to acquire the inputs.

We will now briefly describe conventional transducers for three types of physiological measurements: displacement, temperature and biopotentials. These have been particularly useful in the study of the arterial system. Transducers for

Parameter or measuring technique	Principal measurement range of parameter	Signal frequency range, Hz	Standard transducer or method
Bladder pressure	1-100 cm H_2O	dc-10	Strain-gage manometer
Blood flow	1-300 ml/s	dc-20	Flowmeter (electro-magnetic or ultrasonic)
Blood pressure (arterial) Direct	10-400 mm H_g	dc-50	Strain-gage manometer
Indirect	25-400 mm H_g	dc-60	Cuff, ausculation
(Venous)	0-25 mm H_g	dc-50	Strain-gage
Cardiac output	4-25 liter/min	dc-20	Dye dilution flowmeter
Electrocardiography (ECG)	0.5-4mV	0.01-250	Skin electrodes
Electroencephalography (ECG)	5-300 μV	dc-150	Scalp electrodes
(Electrocorticography and brain depth)	10-5000 μV	dc-150	Brain-surface or depth electrodes
Electrogastrography	10-1000 μV	dc-1	Skin-surface electrodes
	0.5-80 mV	dc-1	Stomach-surface electrodes
Electromyography (ECG)	0.1-5 mV	dc-10,000	Needle electrodes
Eye Potentials			
(EOG)	50-3500 μV	dc-50	Contact electrodes
(ERG)	0-900 μV	dc-50	Contact electrodes
Gastrointestinal pressure	0-100 cm H_2O	dc-10	Strain-gage manometer
Nerve potentials	0.01-3 mV	dc-10,000	Surface or needle electrodes
Phonocardiography (PCG)	Dynamic range 80 dB, threshold about 10^{-4}Pa	5-2000	Microphone
Plethysmography (volume change)	Varies with organ measured	dc-30	Displacement chamber or impedance change
Circulatory	0-30 ml	dc-30	Displacement chamber or impedance change
Respiratory functions Pneumotachography (flow rate)	0-600 liter/min	dc-40	Pneumotachograph head and differential pressure
Respiratory rate	2-50 breaths/min	0.1-10	Strain-gage on chest, impedance, nasal thermistor
Temperature of body	32-40°C 90-104°F	dc-0.1	Thermistor, thermocouple

Figure 3.1 Physiological parameters: measurement and frequency range (from Webster, [30])

measuring displacement are used for determining size, shape and position of organs. For example, they can be used to directly measure changes in the diameter of arteries, or change in volume or shape of cardiac chambers. Displacement-sensitive transducers are also used for indirect measurements. For example, they can be used to detect movement of a microphone diaphragm that detects arterial bruit. An example of a displacement sensitive transducer is the strain gauge. When a fine wire is strained its resistance changes due to the variation in its length and diameter. The inductance of an inductor can also be used to measure displacement by mechanically changing the number of turns of coil, the geometric form factor or the effective permeability of the core. Capacitance between two parallel plates can be changed by varying the distance seperating them. Piezoelectric meterials generate an electric potential when mechanically strained. The piezoelectric effect is commonly used in ultrasonic transducers.

Temperature measurements are useful indices of physiological malfunctions related to blood circulation. For example, decrease in blood pressure of a person in shock causes decrease in blood flow to the periphery which results in changes in skin temperature [17]. Thermocouples are pairs of dissimilar conductors joined so that an electromotive

force is developed by the thermoelectric effect when the temperatures of the junctions are different. Thermistors are devices that exploit the fact the resistivity of semiconductors change with temperature. Radiation thermometry makes use of the relationship between the surface temperature of an object and its radiant power. Thermography has been found useful in determining various circulatory disorders (eg. carotid artery occlusion).

Biopotential electrodes are more than just an interface between the body and electronic instruments. They are transducers since they convert body ionic currents into electrical currents. Chemical reactions at the electrode-electrolyte interface transfers the charges from the cations and anions in the electrolyte and the electrons in the electrode.

Several methods and instruments have been contrived to measure different parameters related to the circulatory system. Invasive methods, in which transducers are placed in the blood vessels, provide accurate information about parameters such as blood flow and pressure. These include electromagnetic flowmeters, intravascular devices and angiography. The electromagnetic flowmeter is based upon Faraday's law of electromagnetic induction, [18]. A magnetic

field is applied across the blood vessels, perpendicular to the flow axis. A potential difference, linearly related to the blood flow rate, is detected by electrodes placed normal to the magnetic field and flow axis. The drawback of this device is that the vessel has to be exposed.

Intravascular devices are used to accurately record the pulse pressure wave. Pressure transducers are surgically inserted inside the blood vessels. This limits their use to cases where the invasion of the blood vessel is justified by the condition of the patient. In angiography a series of x-ray films of a blood vessel is taken in rapid sequence following the injection of a radioopaque substance into the vessel [19]. It is useful for examining the shape and size of various arteries. However, this technique has limited usefulness and carries risks for the patients.

Non-invasive instruments usually provide less reliable information than invasive methods. In plethysmography, information about total flow to a limb is obtained by measuring volume changes in the limb [20]. Venous blood flow is occluded with a pressure cuff. The rate of change of limb volume is therefore related to arterial blood inflow. In electrical impedance plethysmography electrodes are attached to a segment of tissue. Changes in tissue volume due to

blood inflow results in change in the tissue impedance. Phonocardiography is used to detect turbulent flow in occluded arteries. In thermography, changes in regional blood flow are detected by monitoring varations in skin surface temperature distributions.

Ultrasound propagates with different velocities in tissues with different densities and elasticity. This property permits the use of ultrasound in outlining the shape and position of different organs in the body. The ultrasound blood velocity meter is a typical application. Ultrasonic energy (2-5 MGz) is directed obliquely toward a blood vessel. Signals reflected from blood cells are shifted in frequency by an amount proportional to the velocity of the cells, [21].

Ultrasound has also been used to monitor arterial wall motion [22,23,24]. These techniques are however limited to the study of peripheral pulse wave character and peripheral pulse propagation speed.

3.2 THE ELECTROCARDIOGRAPH AND THE MICROWAVE PULSE RECORDER

One of the basic inputs required for our system is an electrocardiograph, which records the ECG. It is basically a

high gain differential amplifier with high common mode rejection and high input impedance. Figure 3.2 shows the diagram of our electrocardiograph. The isolation and protection circuit protects the patient from hazardous currents that could be generated in the electrocardiograph. It isolates the electrode from the electronic circuits and the power line. A calibration signal is usually provided. The preamplifier provides the high common mode rejection and input impedance. A driver amplifier amplifies the ECG to the level of the range of the device that records it (eg. pen recorder or A/D converter). It also usually includes a gain control switch or a programmable gain amplifier.

The microwave pulse recorder (MPR) was first described by Stuchly et al. [1]. A block diagram of the device is shown in Figure 3.3. It consists of a microwave oscillator coupled to an antenna through a circulator. The antenna is an open ended waveguide filled with a dielectric material chosen to provide good matching with the skin. A continuous wave electromagnetic signal at microwave frequencies is transmitted into the body. When the signal meets tissue interfaces having different dielectric properties part of the signal is reflected back to the antenna. The returned signal is then mixed with the original signal using a Schottby barier diode. The transmitter signal may be expressed as

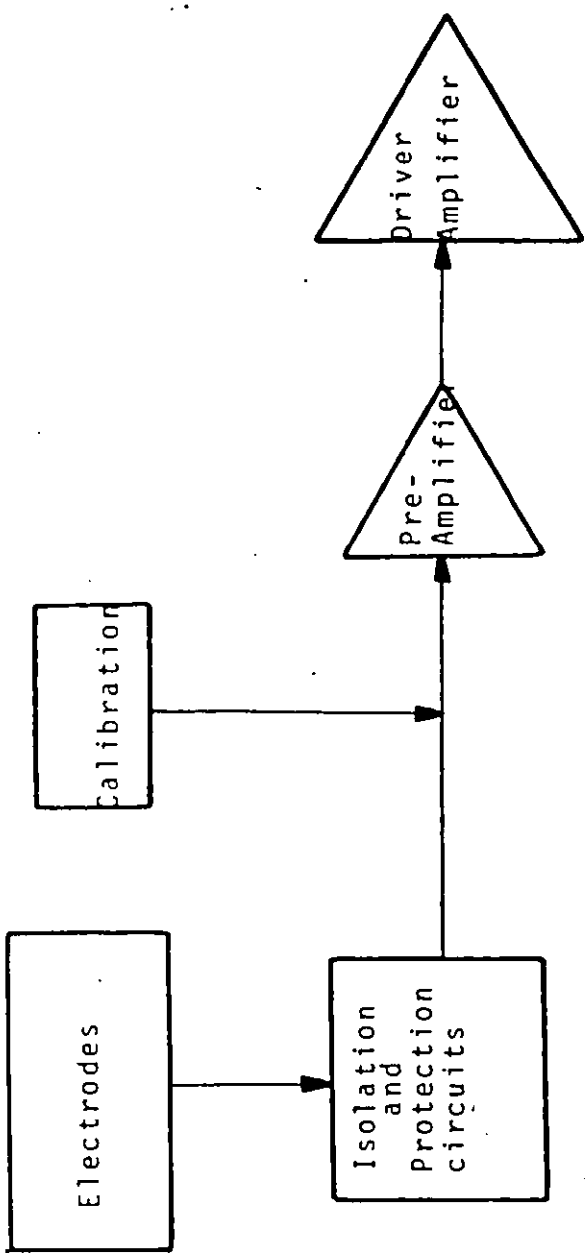

Figure 3.2 Block diagram of our electrocardiograph.

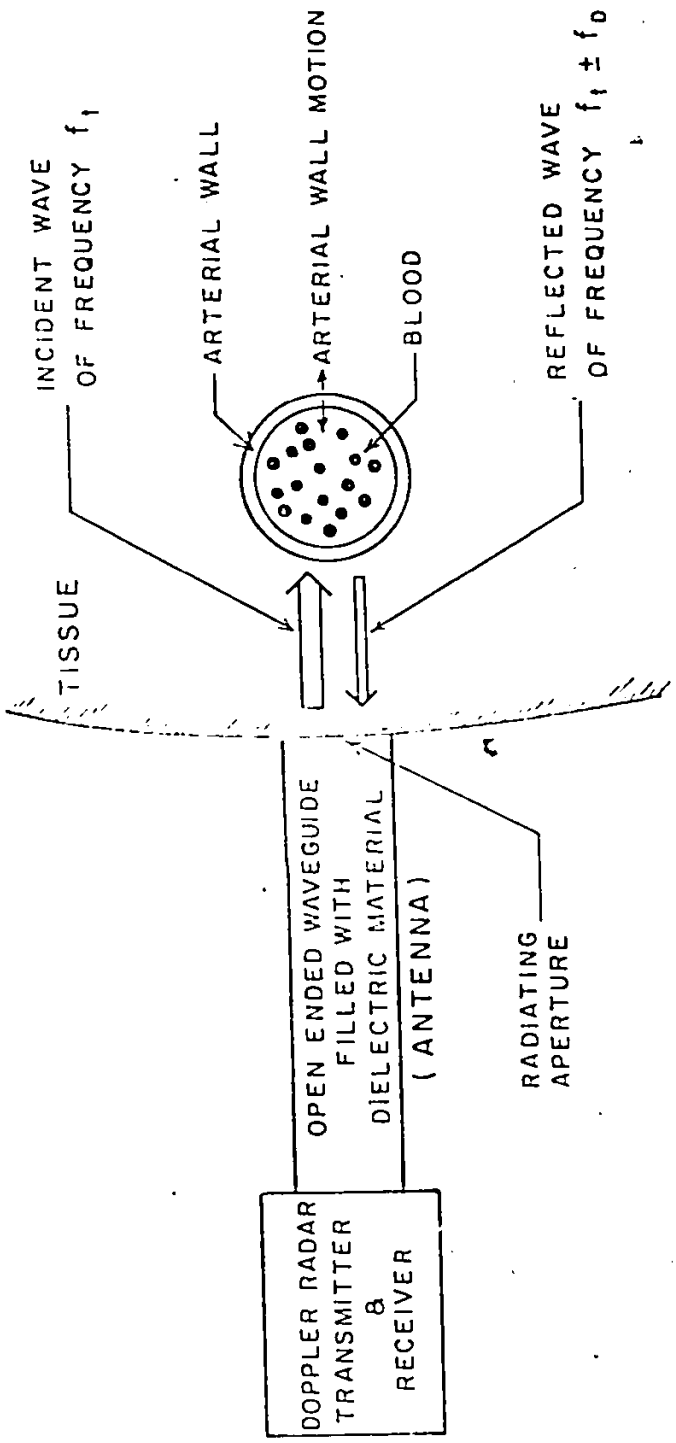

Figure 3.3 Schematic Diagram of the MPR System

$$v_T(t) = V_T \exp[j(\omega_0 t + \theta_T)] \tag{3.1}$$

where V_T, ω_0 and θ_T are amplitude, frequency and phase of the transmitter signal, respectively. The returned signal may be represented by

$$V_R(t) = V_R \exp[j(\omega_0 t + \theta_R(t))] \tag{3.2}$$

where V_R and $\theta_R(t)$ are its amplitude and phase, respectively. The amplitude V_R depends upon V_T, the structure of biological tissues adjacent to the antenna and tissue attentuation characteristics at ω_0.

The signal $V_R(t)$ is heterodyned in the mixer with a portion of the transmitter signal. After filtering unwanted components out, the resulting signal is

$$\begin{aligned} v(t) &= V \cos(\pi + \theta_T - \theta_R(t)) \\ &= V \cos(\pi + \theta_0 + \theta(t)) \end{aligned} \tag{3.3}$$

where V and θ_0 are constants, and $\theta(t)$ is a time-varying phase change. The constant V depends upon the sensitivity of the receiver, V_T and V_R. The constant θ_0 depends upon frequency ω_0 and the structure of the biological tissue.

For a small phase change, $\sin\theta(t) = \theta(t)$, and (3.3) may be rewritten as

$$v(t) = - V\cos\theta_0 + (V\sin\theta_0)\ \theta(t) \qquad (3.4)$$

The output signal is therefore sensitive to phase changes in the reflected signal. If the tissue properties (impedance) varies, the reflected signal will change in phase and magnitude. The detected signal is therefore sensitive to changes in the position of the reflecting interfaces.

The MPR can be used to monitor, non-invasively, arterial wall displacements. However, one major problem encountered with this method is the non-linear behaviour of the detector. Experimental results obtained by Thansandote [25] are shown in Figure 3.4. Using a precision apparatus for measuring the motion of a bovine artery sustaining pulsatile flow of water, he found that as the antenna-artery distance varied the detected signal (i.e. the phase difference) fluctuated around zero. He explains that this phenonmenon occurs because the arterial wall appears to the antenna as a mismatched load resulting in a standing wave which changes the amplitude of the detected phase. The decreasing amplitude of the curve is due to the attenuation of the microwave in water which was used to simulate the biological tissue.

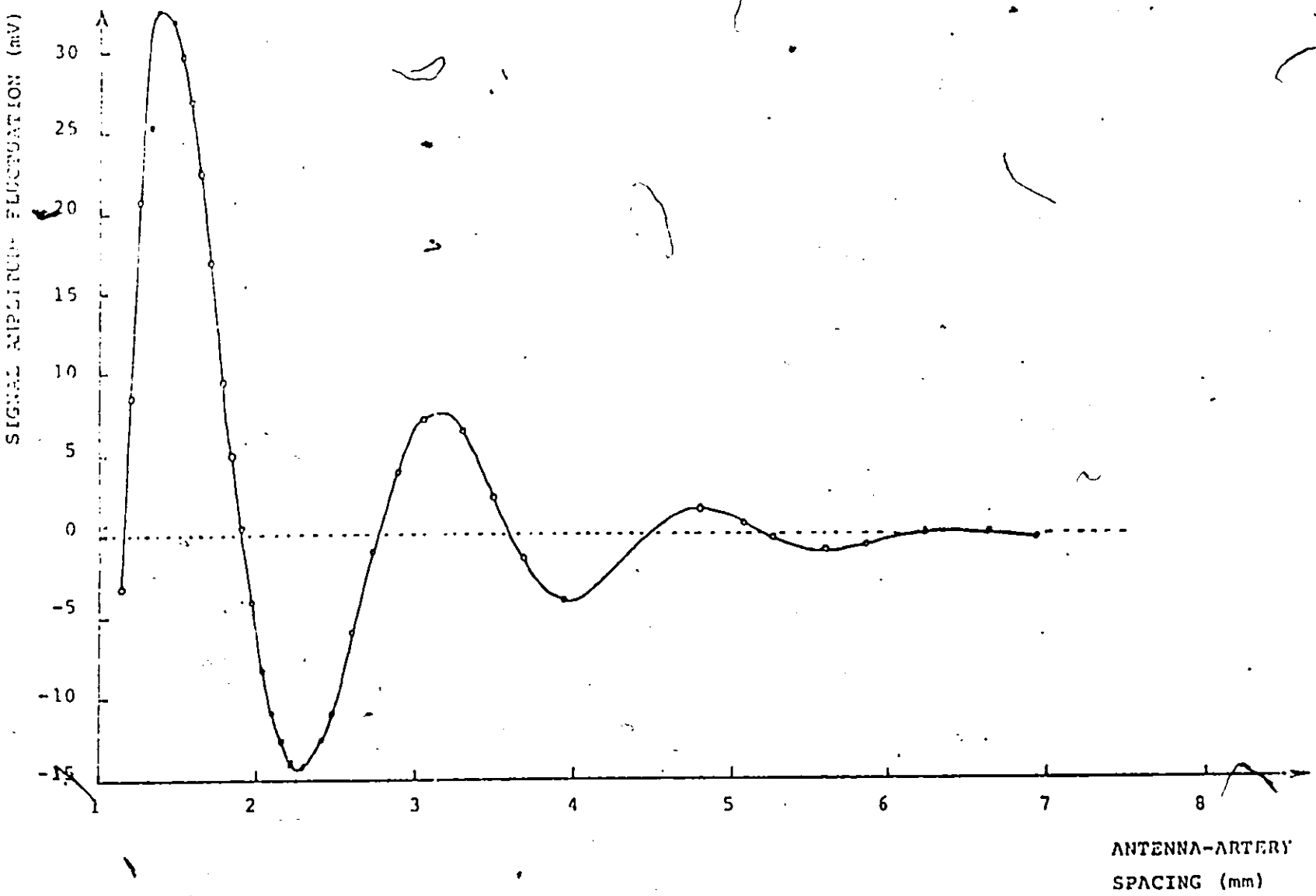

Figure 3.4 Observed variation of MPR signal as a function of antenna-artery spacing (from Thansandote, [25])

Because of the non-linear characteristics and the impossibility to obtain calibrated signals of wall displacement it is presently only practical to extract timing parameters such as the PWV from the detected signals. However, since the penetration depth of microwaves in biological tissue, such as bone, and in air is much greater than for ultrasound, microwaves are well suited to monitor deeply situated arteries such as the aorta and iliac arteries. The attenuation of microwaves in several biological tissues plotted as a function of frequency are shown in Figure 3.5.

In this chapter we have discussed various physiological transducers and given a description of the MPR. The theory for MPR signal processing will be presented in the following chapter.

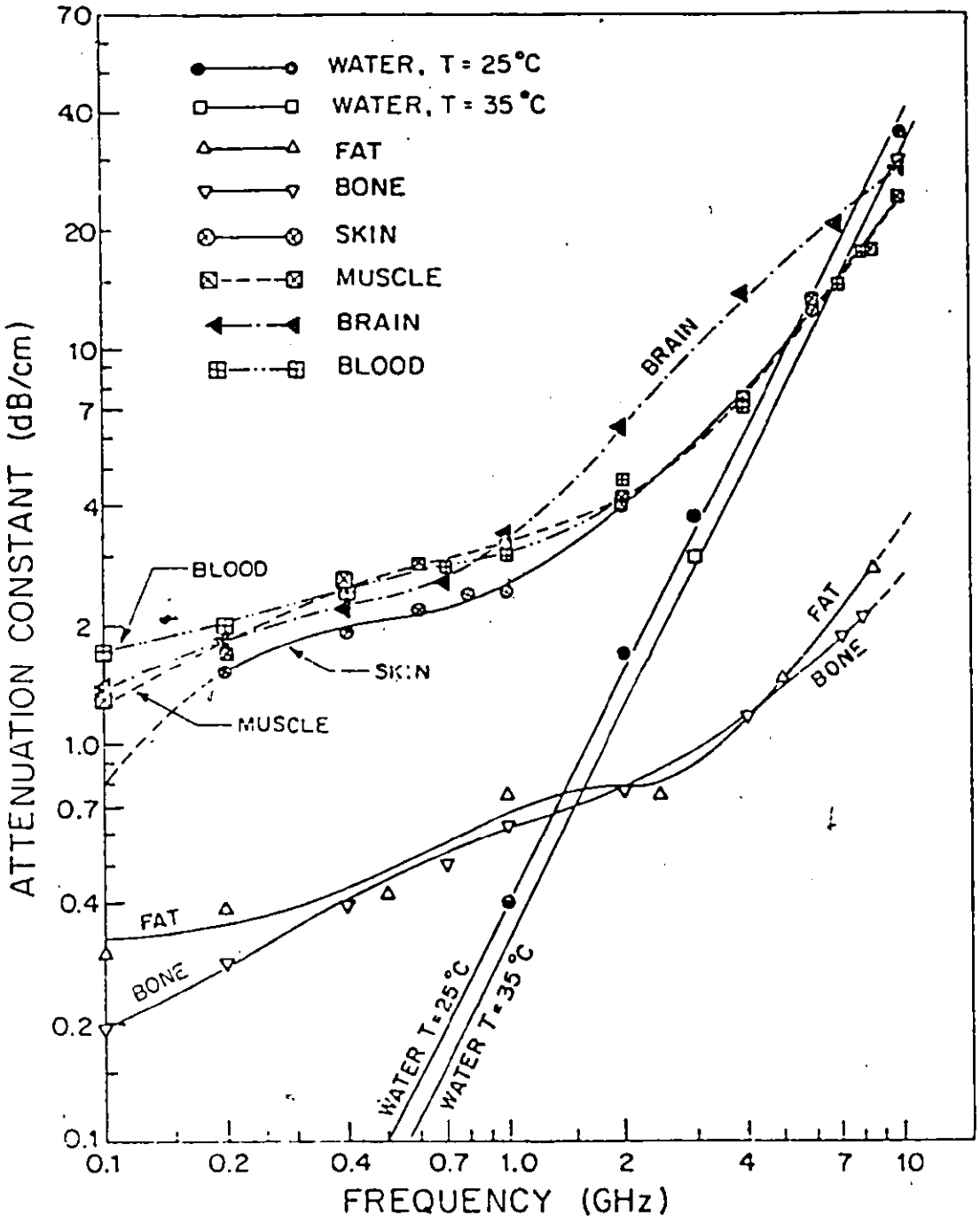

Figure 3.5 Attenuation of microwaves in water and in several biological tissues (from Thansandote, [25])

Chapter IV

SIGNAL PROCESSING THEORY

4.1 SAMPLING AND WINDOWING

Growth and diversification of digital processing equipment are responsible for many modern signal processing applications. In digital signal analysis systems, physical quantities are converted to electrical signals by a transducer. The output of the transducer is then digitized; usually at equal intervals. That is, the analog signal is converted to a sequence of numbers.

Suppose a function f(t) is sampled at equal intervals of T seconds (i.e. fn =f(nT); n= 0,1,2,....). The question arising is how small or large should or can the sampling interval, T, be in order to completely describe f(t) with a sequence of numbers [fn]. To answere this question it is necessary to impose a restriction on f(t). The well known sampling theorem states that to be able to recover f(t) exactly, it is necessary to sample f(t) at a rate greater than twice its highest frequency component [27]. We assume that the function f(t) is bandlimited (i.e. the Fourier

transform vanishes for values of $\omega > \omega c$). It is seen that the Fourier transform of the sampled function $\Sigma f(t)\ (t-nT)$ is periodic with period $\frac{1}{2}$ T and that the individual repetitions can overlap. To avoid this problem it is therefore necessary to select the sampling interval T so that $1/T > \omega c$, or

$$1/2T > fc \qquad (4.1)$$

Thus, if one multiplies the Fourier transform of the sampled function by the function

$$I(\omega) = 1\ , \quad -\omega c < \omega \leq \omega c \qquad (4.2)$$
$$0\ , \quad \text{elsewhere,}$$

it is possible to recover $F(\omega)$ completely; and consequently $f(t)$, the original function.

Of particular importance for our application are the sampling rates required for physiological signals; more specifically the ECG and the blood pressure pulse wave. Signal frequency ranges of various physiological parameters are given in Figure 3.1. From this table, we see that the sampling rates for the ECG and the blood pressure wave should be greater than 500 Hz, and 100 Hz, respectively. Several

other researchers agree with these values [28,29,30].

Another operation to which we subject the data in digital signal analysis systems is windowing. For practicality the data to be processed are N uniformly spaced samples of the observed signal. A finite sampling interval NT can be represented by multiplying the sampled function by the window function

$$w(t) = \begin{cases} 1, & 0 < t < NT \\ 0, & \text{elsewhere.} \end{cases} \qquad (4.3)$$

The multiplication in the time domain translates into convolution in the frequency domain. Since $W(j\omega)$ has frequency components extending to infinity the convolution introduces distortions which are clearly evident in the frequency domain representation of the sampled function. This phenomemon is referred to as spectral leakage. Therefore, even if the sampling theorem is satisfied it is still impossible to completely recover the original function from a finite sampled function.

Windows are weighting functions applied to the data to reduce the order of discontinuity at the boundary of the periodic extension of the data. Harris, [31] and Nutall,

[32] make available concise reviews of some well known data windows. The Hanning and Hamming windows are examples of data windows. The Hanning window is defined as follows

$$w(t) = 0.5(1-\cos(2\pi t/NT)) \quad ; \; 0 < t < NT. \qquad (4.4)$$

The Hamming window is a modified Hanning window which gives a marked improvement in sidelobe levels. It is given by

$$w(t) = 0.538 - 0.462 \cos(2\pi t/NT) \; ; \; 0 < t < NT. \qquad (4.5)$$

The selection of a data window is dictated by the particular requirements, in terms of bias due to nearby sidelobes and bias due to distant sidelobes in their frequency spectrum.

Also important is the width of the main lobe. Ideally the data window should be of infinite length. This corresponds to an impulse in the Fourier domain. The Fourier transform of the window function should, therefore, approximate an impulse.

4.2 SAMPLING AND QUANTIZATION

Noise associated with undersampling and windowing were discussed in the previous section. There are other sources of noise associated with sampling and analog to digital

converters (ADC). An ideal sampling process implies that a signal is sampled at equal intervals; that is, the value of each sample is equal to the amplitude of the signal at the sampling time. If the sampling process is unstable in time the signal will be sampled at a time other than that assumed, resulting in an error proportional to the rate of change of the signal. This error is referred to as jitter noise.

Sampling continuous signals implies that we are representing voltage levels by numerical values stored in binary format. For an n-bit binary word it is possible to represent 2^n different voltage levels in a specified voltage range. Signal levels between these steps will be undetected. These errors are referred to as quantization noise.

If we assume that the step size S is small in comparison with the peak to peak range of the analog signal, we can assume that the probability density function of that signal is constant within each quantization step. In this case it can be shown, [33], that the mean squared error is given by

$$e^2 = S^2/12 \qquad (4.6)$$

The step size is

$$S = Vr/(2^n-1) \qquad (4.7)$$

where Vr is the peak to peak range of signal and n is the number of bits in the binary word. If we assume a uniform distribution of the signal voltage the mean squared signal V^2 is given by

$$V^2 = Vr^2/12 \qquad (4.8)$$

The signal to noise ratio (SNR) is therefore

$$SNR = V^2/e^2 = 2^{2n} \qquad (4.9)$$

Thus if we have an ADC with 12 bits of resolution the device has 72 dB of instantaneous dynamic range based on quantization noise alone.

4.3 OTHER SOURCES OF NOISE

An important source of noise is the constant agitation at the molecular level. This agitation of molecules is called thermal agitation since it increases with temperature. For example, in resistors, there exists random wanderings of electrons. This causes a voltage difference between the

resistor terminals. This is referred to as resistor thermal noise. A second type of noise shot noise results from a phenomenon associated with the flow of current across semiconductor junctions. Thermal noise has a quasi-uniform power spectral density up to frequencies of the order of 10^{13} Hz. Shot noise has a power spectral density reasonnably constant up to frequencies of the order of the reciprocal of the transit time of charged carriers across the junction.

4.4 FILTERING THEORY

A filtering process involves the elimination of bands of frequencies. Digital filtering is used for signal smoothing, noise rejection, signal reconstruction and feature extraction. For our application an essential characteristic of the filter is that it should not introduce non-linear phase shift. For this reason only non-recursive filters are discussed. The transfer function of a non-recursive filter is given by

$$H_N(j\omega) = \sum_{n=-N}^{N} bn \exp(-j\omega nT) \tag{4.10}$$

where $H_N(j\omega)$ is expressed as the discrete Fourier transform (DFT) of a function b(t) having the samples [bn].

The synthesis of non-recursive filters involves the selection of a set of filter coefficients [bn] to achieve a desired frequency response. Coefficients can be derived such that $H_n(j\omega)$ is a least squares approximation to $Hd(j\omega)$, the desired transfer function. The coefficient equation, [27], is given by

$$bn = (T/2\pi) \int_{-\pi/T}^{\pi/T} Hd(j\omega) \exp(jn\omega T) \; ; \; -N < n < N \qquad (4.11)$$

The closeness of the approximated transfer function, $H_N(J\omega)$, to the desired transfer function, $H_d(j\omega)$, obviously increases with N.

4.5 INTERPOLATION AND DECIMATION

Interpolation and decimation are basic processes in digital signal processing. They are used when conversion from one sampling rate to another is required. For example decimation is used to reduce the number of samples of a signal to be stored or transmitted. Interpolation is often used for reconstructing signals from a low bit rate representation. Interpolation and decimation techniques are also useful for defining efficient implementations of narrow band non-recursive filters [34].

The design of interpolation or decimation processes involves the use of lowpass (or bandpass) digital filters. We will briefly outline the effect of different interpolating functions by first considering the process in the Fourier domain.

As noted previously, the Fourier transform of a sampled function fs(t) is a periodic repetition of the transform of the original function f(t). Thus, given $Fs(\omega)$, we have

$$F_r(\omega) = Fs(\omega)\ I(\omega) \qquad (4.12)$$

where $I(\omega)$, defined by equation (4.2), is the interpolating function, and $F_r(j\omega)$ is the Fourier transform of the reconstructed function. In the time domain we have

$$f_r(t) = fs(t) * F^{-1}[I(\omega)] \qquad (4.13)$$

where $$F\ [I(\omega)] = \sin(\pi t)/\pi t \qquad (4.14)$$

This is the ideal interpolator. However, it is inpractical since it decays to zero very slowly. It is possible to approximate (4.14) by truncating it to n points.

There are several other approximations to the optimum interpolator. One approach consists in approximating the

interpolation function with a set of polynomials (splines). Another approach consists in multiplying the sinc function by $(1-x^2/n^2)$ in order to remove the discontinuities produced by truncation, [26].

The accuracy of an interpolator can be estimated in terms of the autocovariance of the unsampled signal. The mean squared error is given by

$$e(t) = E\left|fr(t) - f_s(t)\right|^2 \qquad (4.15)$$

where $fr(t)$ is the reconstructed signal, and $f_s(t)$ is the sampled signal.

It can be shown, [35], that

$$e(t) = C(0) - 2\sum_{i=o}^{n} C(t-i)I(t-i) + \sum_{i=o}^{n}\sum_{j=o}^{n} C(i-j)\, I(t-i)\, I(t-j) \qquad (4.16)$$

where $C(t)$ is the autocovariance of $f(t)$ given by

$$C(t) = E[f(t+t)f(\tau)] - E[f(t+\tau)]\, E[f(\tau)] \qquad (4.17)$$

4.6 PULSE WAVE VELOCITY MEASUREMENT

There are several approaches for measuring the PWV from the MPR signals. The problem consists in extracting certain features from the signals at different locations on an artery in order to estimate the time delay between them. McDonald [14] used a cross-correlation technique in which one of the signals is shifted across the other and the correlation coefficient is computed. The shift position at which the correlation is maximum is defined as the time delay between the two signals. This method is rather accurate since it filters out problems caused by signal distortions. It is, however, quite involved computationally and is therefore inpractical for real time PWV measurements.

Another method consists in identifying a stable time reference point on the waves. One such point can be the peak of the MPR signal. The problem then becomes one of function minimization (or maximization). If a function f(t) is differentiable in an interval [a,b], a necessary condition to have a local minimum (note that when we consider minima we can equally consider maxima) at a point $m \varepsilon (a,b)$ is $f'(m) = 0$. One way of solving this is by approximating f' numerically (eg. by finite differences) and searching for a zero of f'.

In this chapter we have presented digital processing techniques required for this project. In the following chapter we present an overview of hardware required for the CSR.

Chapter V

DIGITAL HARDWARE CONSIDERATIONS

In the previous chapter we have discussed digital signal processing theory relevant to the CSR system. In this chapter we will examine digital hardware available to perform the described signal processing functions.

5.1 ELEMENTS OF DIGITAL SYSTEMS

Digital processing presents many advantages over signal processing using discrete analog components. The digital processing approach eliminates the need for component matching and system re-tuning often required for analog circuits since digital components behaviour is stable, predictable and repeatable, [27]. Digital processing also eliminates costly precision components and signal degradation due to circuit interaction with noise.

The use of programmable digital components, such as microprocessors, permits greater flexibility for modifications, improvements and addition of extra features. The basic elements of a digital signal processing system consists of an anti-aliasing filter, a sample and hold

amplifier (SHA), an analog-to-digital converter (ADC) and a digital processor. The anti-aliasing filter is used to bandlimit the analog signal to eliminate aliasing noise. The filtered signal is then sampled at a rate determined by the digital processor. The SHA is used to hold the signal long enough for the analog-to-digital conversion. The ADC is then used to convert a sample into a digital word. The main component of the digital processor is a central processing unit (CPU) which inputs and outputs data and carries out logical and arithmetic operations under the directions of a program. Other processor elements include program and data memory as well as other electronic components to direct internal data flow and control peripherals devices such as input keyboards and output displaying and storage devices.

5.2 MICROPROCESSORS IN MEDICINE

The number of biomedical applications of microprocessors have considerably increased in the last few years, notably in cardiology and physiology. The decision making capability incorporated by the microprocessor in the instruments significantly increases the degree of automatism and considerably simplifies the man-machine interface. At first microprocessors were used primarily as process controllers. Advancement of microprocessor technology in the areas of

power efficiency and speed have however contributed to the increased useage for their computing capabilities. The main advantages of using microprocessors is that they require less components and are programmable. The benefits of having less components are: reduced volume, hence portability of the system; reduced power consumption and dissipation; smaller number of interconnects resulting in increased reliability; and lower cost. The advantages of programmability are that design is simplified and that the development time is reduced.

In biomedicine, the computing capability of the microprocessor is found useful in many applications since the data rates are low enough for the microprocessor to be able to acquire, process, and then store or display the bio-signals, [36]. Some of the latest ECG instruments use microprocessors to incorporate intelligence in order to diagnose some heart defects or to warn about abnormal heart rythms, [37]. Numerous other applications include the following: beside monitoring of patient circulatory, respiratory, and central nervous systems, as well as metabolic and acid/base control systems; feedback control of the breathing of bed patients and the automatic infusion of intravenous fluids; automatic chemistry analysers which allow blood counts to be made by relatively unskilled personnel, [38].

In microprocessor based systems the processing unit is the cheapest resource in the system. It is therefore an error to time share the processor amongst several tasks. The most efficient solution is to dedicate a processor to a process since the complex executive to supervise multi-tasking is not required. These single process dedicated processor systems are referred to as distributed systems, [39,40]. In contrast with multimicroprocessor systems, distributed systems do not truly interact with each other for control purposes in real-time, but only exchange data. Distributed systems usually consist of a main "master" processor with one or more "slave" processors. True multimicroprocessor systems usually require complex operating systems to synchronise the overall system activities. For that reason it is not cost-efficient to implement multimicro-processor systems using monolithic microprocessors.

In distributed or multimicroprocessor systems, two or more microprocessors can be interconnected using several methods including memory communications, inter-register communication and direct-bus intercommunication. With dual-microprocessor systems the memory communication scheme can be achieved by using dual ported RAM's. With this approach, access priority are determined by having a port with higher priority. A lock mechanism is also required to control the

access of the memory (i.e. to protect against simultaneous read and write). Another approach which is cheaper and usually faster consists in having two single ported memory blocks switched between the two microprocessors. This block sharing mechanism is particularly efficient when a microprocessor can independantly process a block of data and then turn over that block to the other processor for further processing. Inter-register communication involves the use of interface chips such as the programmable input-output (PIO). The shared register is in an I/O register in the PIO. These systems are usually interrupt driven and are most efficient for word-oriented communication. This scheme is however quite slow for block-oriented transfers.

5.3 SPECIAL PURPOSE DIGITAL HARDWARE

In biomedical applications the communication between the processing unit and the outside world is of considerable importance. As with standard computers, devices can interrupt microprocessor to request servicing. Most microprocessor manufacturers supply I/O management chips to support their microprocessors. For example, programmable interrupt controller (PIC) allow standard microprocessors to handle several interrupt lines. The PIC can manage multiple interrupt priorities and implement automatic interrupt

vectoring. Many microprocessor vendors also supply memory management hardware units (MMU) to handle memory mapping in complex distributed processor systems.

Many biomedical applications require long time delays (a few milliseconds). Software timing loops are therefore inefficient in many applications where the processor time is needed to perform other functions. The programmable interval timer (PIT) considerably improves the amount of processor time to perform other tasks. It can be used to measure time differentials between events or event durations. As output it can be used as a time counter to generate programmed delays for real time process control.

Many inherent I/O problems can be solved by using an intelligent I/O subsystem which isolates the CPU from the peripheral devices. For example, the INTEL 8089 I/O processor (IOP) can be used to control all I/O operations, under the supervision of the CPU. The IOP performs device initialization, record selection, I/O transfer, simple data transformation, error checking and retries, and signals the CPU upon the successful completion of the I/O transfer. The CPU and the IOP communicate through the system memory. The CPU signals the IOP for servicing, the IOP then reads the memory and performs the appropriate I/O operations. I/O

tasks such as CRT screen refresh, CRT buffer update, floppy disk transfers and keyboard scan and decode can be dedicated to the IOP thus significantly improving the system throughput.

Another useful I/O management device that speeds up word and block transfers between memory and I/O devices is the direct memory access controller (DMAC). The DMAC implements transfer algorithms in hardware. When the DMAC is interrupted by an I/O device it sends an "Hold" signal to the CPU and performs the transfer operation at hardware speeds. DMAC's are typically used in the case of fast I/O devices such as disks or CRT's. They, however, contribute conside rably to a system's cost and are, therefore, not used with small systems.

There exists several special purpose multiplier chips which permit microprocessor implementation of algorithms that require the extensive computation of products and sum of products. Depending upon the techniques used to input and output data from and to the hardware multipliers, increases in multiplying speed by factors of 10 to 25 can be achieved.

In this section, we have presented many useful components and functions for assembling microprocessor

systems. In the next section, we will give a brief overview of various mass storage devices most often used with microprocessor systems to store biomedical data.

5.4 MASS STORAGE DEVICES

Mass storage devices, or secondary memories, fall into two categories: sequential and random access devices. Sequential devices permit reading and writing in fixed sequences only, [41]. Most common sequential devices used with microprocessor systems are magnetic tapes as well as cassettes and tape cartridges. These devices write and read data in block format and are therefore best suited for applications where data is organized sequentially or accessed only occasionally. Because these mediums are so inexpensive they are attractive for storage of large quantities of data. They are however relatively slow. Information is recorded at densities of 800, 1600 and 6250 bpi and transfer speeds range from 15 ips to 200 ips. At 1600 bpi this is the equivalent of 24 kbauds at 15 ips and 32 kbauds at 20 ips. The speeds are, however, fast enough for many biomedical applications where data is stored in real time.

Random access devices are used to permit direct or pseudo-random access to specified data. They are faster than

tape systems but are also much more expensive. Magnetic disks are typical random access devices. The floppy disk or diskette, because of its low cost, is extensively used with microcomputer systems. A single density, single sided diskette can hold about 250 kbytes of data. Double density, double sided diskettes can hold up to 1 Mbyte of data. Also, recent increases in sales of personnal computers have led to decreases in costs of floppy disk drives.

Two relatively new memory technologies show great potential for microcomputers. These are charged couple devices (CCD) and magnetic bubble memories, [42]. If successful, these technologies could replace fixed head disks since they offer more speed and greater capacity at a lower price. CCD's offer very high density data storage. One Mbit memories on 50 mm chips should be available in a few years. Magnetic bubble memories achieve data rates comparable to rotating storage devices but at a much lower cost with reliability not achieveable by mechanical devices. Even though the technology to produce bubble memories is simple in principle, there have been some problems with obtaining high yields from the available material. Magnetic bubble devices currently operate at data rates of about 50 kbauds and have storage capacity of about 20 Kbytes.

In this chapter we have presented a brief overview of digital hardware commonly used in microcomputer systems with emphasis on biomedical applications. In the following chapter we will present a simulation system demonstrating the performance of the signal processing algorithms and justifying the implementation of the Cardiovascular Signal Recorder.

Chapter VI

CSR SYSTEM SIMULATION

In this chapter we will present the development of a CSR simulation system which will enable us to predict the performance of a microprocessor based CSR system and to study the effects of certain parameters on our measurements. The information will also serve in evaluating the potential and limitations of the CSR design. We will first establish a number of basic goals for the CSR and then proceed to implement the simulation of the CSR using a microcomputer development system. We will then be able to compare experimental measurements with theoretical uncertainties and try to explain errors if we had not predicted them.

6.1 CSR DESIGN GOALS

After reviewing medical litterature it became apparent that potentially useful applications of the MPR are in determining pulse transit times (PTT) and pulse wave velocity (PWV) in arteries. The PTT can be used as an indication of beat to beat changes in blood pressure while the PWV is a more useful indicator of arterial wall dynamic and arterial

physiological state. The initial goal for this project was, therefore, to develop a portable, easy to operate, system to determine accurately PTT and PWV in different arteries in real time. Since only one MPR device was available it was decided to build the simulation system to measure directly only PTT's. For reasons given in chapter 5, it was decided that the system would be microprocessor based. The CSR could become a useful research tool for monitoring PTT's and PWV's in human arteries.

The CSR microcomputer system functions were initially devised as follows:

1. Signal acquisition control.
2. ECG R-wave detection.
3. MPR signal event detection.
4. MPR signal artifact detection (due to patient motion for example).
5. Data conditioning (e.g. filtering).
6. Computation of PTT, PWV, statistics, and result displaying.
7. Data storage (for later more complex processing).

6.2 PTT AND PWV MEASUREMENT UNCERTAINTY ANALYSIS

In this section, we will analyse the uncertainty on both

the PTT and PWV measurements. From this we will be able to specify the accuracy of basic measurements and help in establishing important system design parameters and requirements.

Three major components contribute to the uncertainty in time measurement for the determination of PTT and PWV:

1. Quantization size
2. Finite sampling interval
3. Statistical system noise

In the analysis, we will assume that the noise component, ΔN, can be virtually eliminated by suitably low pass filtering the ECG and MPR signals. For the PTT measurement the absolute uncertainty, ΔPTT, is equal to the uncertainty in the R-wave to peak MPR signal time measurement, ΔTRP.

ΔTRP depends on the following:

1. ΔPM - uncertainty in peak detection algorithm
2. ΔRW - uncertainty in R-wave detection algorithm
3. ΔQTM - effect of quantization error on MPR peak detection

4. ΔQTR - effect of quantization error on R-wave detection

5. ΔSTM - effect of finite sampling rate on MPR peak detection

6. ΔSTR - effect of finite sampling rate on R-wave detection

We will assume that the R-wave and MPR peak detection algorithm are accurate to one sampling interval (i.e. ΔPM = 0, ΔRW = 0). Since the QRS complex of the ECG is very dynamic, 8 bits per sample quantization is sufficient for reliable R-wave onset detection [11]. We may therefore assume that ΔQTR < ΔSTR. Thus, two cases may occur;

Case 1. $\Delta QTM > \Delta STM$; then $\Delta PTT = \Delta QTM + \Delta STR$ (6.1)

Case 2. $\Delta QTM < \Delta STM$; then $\Delta PTT = \Delta STM + \Delta STR$ (6.2)

The absolute uncertainty due the quantization noise, ΔQTM, depends on the slope of the signal near the peak. That is, if

$$df/dt > \Delta Q / \Delta S \qquad (6.3)$$

in the sampling intervals immediately before and after the peak, then ΔQTM < ΔSTM. It is desireable to find a quantization size for which ΔQTM is always less than ΔSTM. To study the effect of quantization on peak MPR detection accuracy an equation for a portion of the MPR signal was obtained by fitting a cubic polynomial through 20 points around the peak of a MPR pulse digitized at a 2KHz sampling rate. (i.e. 10 ms window around the peak). The resulting curve enabled us to estimate the time uncertainty as a function of quantization size. The results are shown in Figure 6.1. Clearly, at least 12 bit per sample quantization is required for the MPR signal.

Similarly, the ECG signal was digitized and analysed. It was found that the quantization error at 8 bit per sample was neglible compared to the sampling interval (i.e. 0.2 ms). Thus, if the MPR signal is quantized to 12 bits, the absolute uncertainty for the PTT is given by:

$$\Delta PTT = \Delta STM + \Delta STR \; ; \; \Delta STM, \Delta STR > 1.2 \text{ ms} \qquad (6.4)$$

Similarly the uncertainty for the PWV measurement can be derived as follows. The PWV is given by

$$PWV = D / T \qquad (6.5)$$

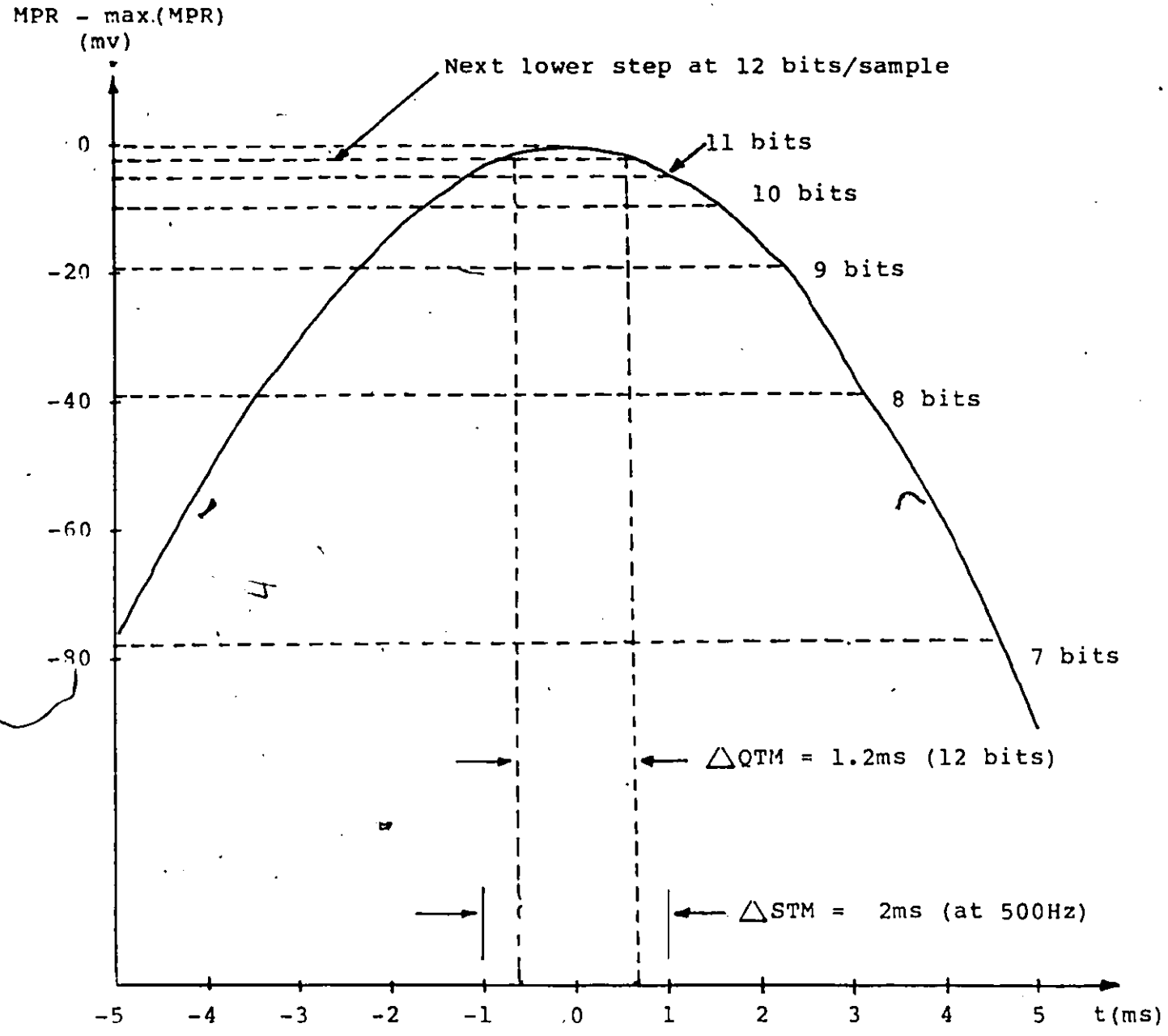

Figure 6.1 Portion of MPR signal centered around the detected peak

where D is the distance between two MPR devices placed along an artery and T is the time differential measured between the peaks of the two MPR signals. Then, it follows that the relative uncertainty for the PWV is given by

$$\frac{\Delta PWV}{PWV} = \frac{\Delta T}{T} + \frac{\Delta D}{D} \qquad (6.6)$$

The absolute uncertainty can be expressed as follows:

$$\Delta PWV = PWV\ (2\ \Delta STM / T + \Delta D / D) \qquad (6.7)$$

Since $T = D/PWV$ and $\Delta STM = 1/f_s$ (f_s= sampling frequency)

(6.7) can be rewritten as

$$\Delta PWV = PWV\ (\ 2\ PWV/Df_s + \Delta D/D)\ ;\ f_s > 1/1.2 \qquad (6.8)$$

6.3 UNCERTAINTY CASE STUDY

6.3.1 PTT MEASUREMENT

Here it will assumed that both the ECG and the MPR signal are digitized at a 500 Hz sampling rate and that the ECG is quantized to 8 bits and the MPR signal to 12 bits.

The uncertainty for the PTT is given by equation (6.4). We also have $\Delta STM = \Delta STR = 1/f_s$. Therefore, we have $\Delta PTT = 2/f_s = 4ms$.

The relative uncertainty on the PTT measurement depends on which artery is being measured. Approximate values, obtainted from estimations of PTT in arteries assuming PWV of 10 mm/msec, are shown below:

radial artery: $\Delta PTT/PTT = 2 / 300f_s = 1.3\ \%$

femoral artery: $\Delta PTT/PTT = 2 / 250f_s = 1.6\ \%$

abdominal aorta: $\Delta PTT/PTT = 2 / 175f_s = 2.2\ \%$

The worst case of 2.2% uncertainty on the PTT measurement seems to be acceptable since significant physiological variability of PTT's should be considerably higher.

6.3.2 PWV MEASUREMENT

In the second case study it will be assumed that the PWV is to be measured over a 200 mm artery segment. Assuming that two MPR devices can be positionned to an accuracy of 5 mm, and that the PWV is 10 mm/ms, and that the MPR's are sampled at 500 Hz and 12 bits per sample, from equation (6.8) we have:

$$\Delta PWV = 10\ (2*10\ /\ (200*0.5) + 5/200) = 2.25\ mm/ms$$

This represent at 22.5% uncertainty on the PWV measurement, which is totally unacceptable. Clearly, for PWV measurements, either the sampling rate needs to be increased or the uncertainty reduced below that of the sampling intervals.

6.3.3 DECREASING THE UNCERTAINTY

In the previous sections it was shown that the uncertainty on PTT and PWV measurements were dependant on the sampling frequency f_s. Tests conducted by Benson, [27], showed that a 500 Hz sampling rate was acceptable for ECG signals. This is also true for pulse pressure signals since they contain even less harmonics than the ECG. It should be possible to increase the resolution of the MPR peak time detection since we are able, in theory, to reconstruct exactly the MPR signal if it is sampled at a rate satisfying the sampling theorem. As discussed in section 4.5, reconstruction of the original signal is achieved by convolving an interpolating function with the sampled signal. Thus, to decrease the uncertainty on the MPR peak occurence, ΔSTM, and the ECG's R-wave onset, ΔSTR, we only need to interpolate the signal around the detected peak and re-evaluate the peak from the resampled signal.

Using equations (4.16) and (4.17) it was possible to estimate the accuracy of several resampling functions for MPR and ECG data. The four point sinc function was found satisfactory for both the MPR signal (average mean squared error of 0.102) and the ECG signal (average mean squared error of 0.096). Since the mean squared error for 12 bit quantization is 0.124, it follows that $\Delta QTM > \Delta STM$ is true if we resample to, say, four times the original sampling rate (i.e. $\Delta STM = 0.5$ ms). From the results in figure 6.1 it follows that

$$\Delta PTT < 1.2 \text{ ms} \tag{6.9}$$

and,

$$\Delta PWV < PWV \left(2.4/T + \Delta D/D \right) \tag{6.10}$$

For D = 200 mm and PWV of 5 mm/ms, 8 mm/ms and 10 mm/ms, the relative uncertainties are 8.5%, 12% and 15% respectively. If better accuracy is required for PWV measurements then a different approach should probably be taken. For example, a correlation method would probably yield results with better accuracy, [14]. Nevertheless, it will be assumed that meaningful physiological variability of PWV's exceeds 15%.

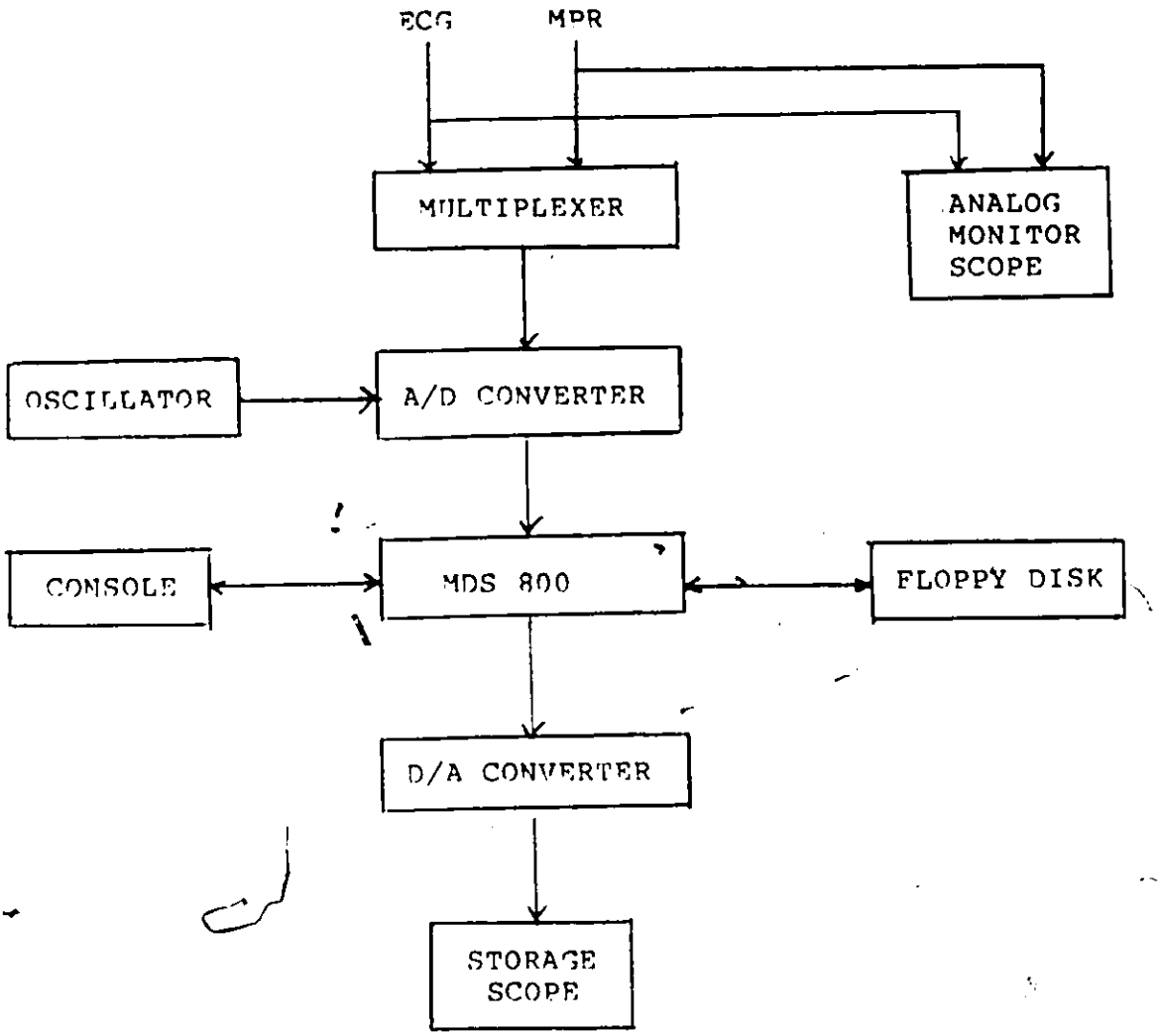

Figure 6.2 Block diagram of CSR simulation system

6.4 CSR SIMULATION SYSTEM DESCRIPTION

6.4.1 GENERAL DESCRIPTION

The general configuration of the CSR simulation hardware is shown in Figure 6.2. The MPR and ECG signals are fed into a MDS800 microcomputer system which consists of an 16-channel multiplexer, a 12-bit A/D converter, a storage scope, a console and two floppy disk drives. The ECG and microwave signals are digitized and are simulataneously displayed on the storage scope. Since the MDS800 is based on a 8080 microprocessor, it has a relatively long cycle. Real time beat by beat analysis was therefore not possible and only every other beat could be processed.

At the beginning of a processing session the operator is prompted for the number of beats to be processed. At the end of the analysis the R-wave to peak MPR pulse transis time (PTT), and statistics such as means and variances are displayed on the console. The R-wave and peak MPR locations are indicated on the storage scope as vertical lines.

6.4.2 DATA FILTERING

In order to remove high frequency random noise from the ECG and MPR signals, a non-recursive digital filter was designed. From the coefficient equation (4.11) $H_n(j\omega)$, the filter transfer function, is made a least square approximation to the desired square box filter, $H_d(j\omega)$, shown in Figure 6.3. The filter coefficient equation is therefore given by

$$b_n = b\text{-}n = T/\pi \int_0^{\pi/T} H_d(j\omega)\cos n\omega t d\omega \qquad (6.11)$$

Here $H_d(j\omega)$ is symmetrical (i.e. real) so that there is zero phase shift.

It follows that

$$b_n = b_{-n} = T/\pi \int_0^{\pi/T} H_d(j\omega) \cos n\omega_c T \, d\omega$$
$$= \omega_c T \frac{\text{sim } n\omega_c T}{n\omega_c T} \qquad (6.12)$$

A better approximation to $H_d(j\omega)$ is obtained by multiplying the sample set $[b_n]$ by the Hanning data window $[X_n]$ given by

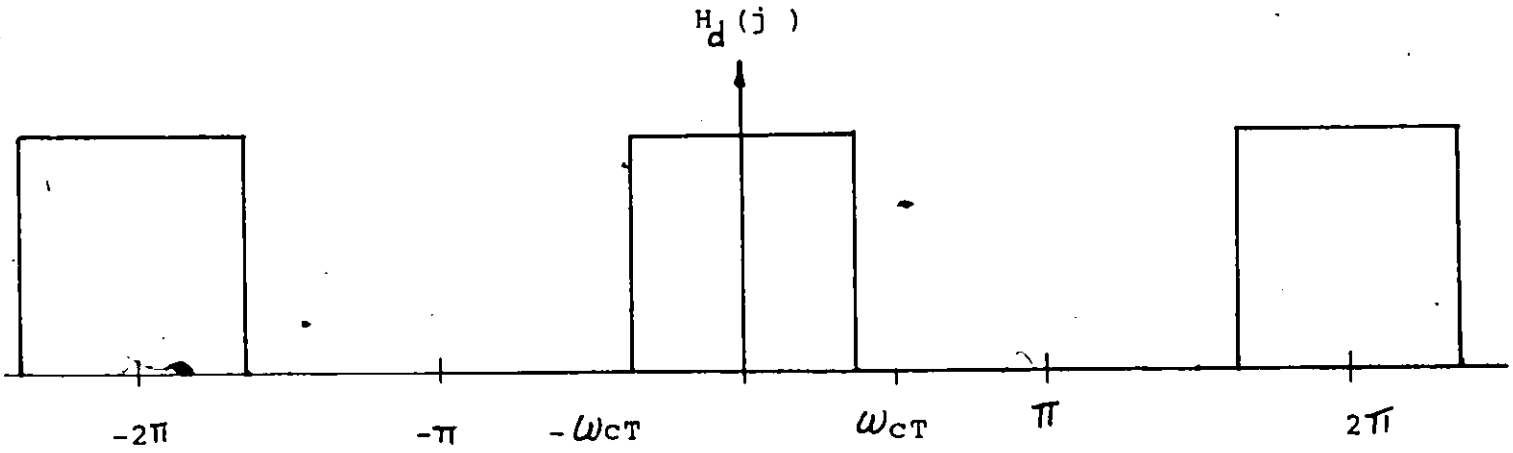

Figure 6.3 Ideal low pass filter

$$X(T) = \tfrac{1}{2}\,(1 + \cos(t\pi/NT)) \qquad (6.13)$$

The modified coefficients are then

$$(bn)\,(Xn) = \frac{(1 + \cos(n\pi/N)\sin n\omega c\, T;\ -n<N<n}{2n} \qquad (6.14)$$

The filter and transfer function formulas are then given by:

$$gm = \sum_{n=-N}^{N} bn\ Xn\ fm-n \qquad (6.15)$$

$$H(j\omega) = bo + 2\sum_{n=1}^{N} bn\ Xn\ \cos n\omega T \qquad (6.16)$$

where gm is the filtered signal at m, and

f_i is the filtered signal at i.

At the beginning of a session the $b_m\ X_m$ coefficient are evaluated for all n values and stored in memory. The filter with N = 2 was used. This requires five multiplications and five additions per sample.

6.4.3 ECG R-WAVE DETECTION

Location of the R-wave is accomplished by finding a point in the ECG data where the absolute value of the first

derivative exceeds a preset threshold.

A least square estimate of the first derivative is obtained from

$$d(i) = \frac{-2f(i-2) - f(i-1) + f(i+1) + 2f(1+2)}{10\Delta t} \qquad (6.17)$$

where the f(i)'s are the filtered ECG samples, Δt is the sampling interval (i.e. 2ms at 500 Hz), and d(i) is the value of the first derivative at the ith sample.

At the beginning of a processing session the first 5 seconds of the ECG data is scanned to locate the maximum of the first derivative. The derivative threshold is then set at 50% of this maximum value. A new dynamic threshold value is then updated every heart beat using the latest 5 beats.

6.4.4 MPR EVENT DETECTION

Artifacts due to patient motion are detected when the absolute value of the first derivative of the MPR signal, computed using equation (6.17), is higher than a certain threshold. When such an event is detected the processing of the current pulse is aborted. The threshold is initially set

to 70 mv/ms which was established through experimentation. This threshold is then periodically updated to be 130% of the maximum absolute derivative of the latest five artefact free pulses.

The search for the peak MPR signal is started a preset period of time after the ECG's R-wave is detected. This time period depends upon which artery is being studied. For example when monitoring the radial artery, the time period is set to 200 ms which is the minimum possible value for PTT. The peak MPR signal is then defined as the first critical point from the start of the search. Depending upon the sign of the first derivative at the beginning of the search, the peak is detected when at least ten consecutive opposite sign derivatives occur.

ECG amd MPR signals are resampled to four times the original rate using the truncated sinc interpolator. This however is only done for samples around the detected R-wave and MPR peak. The same R-wave and MPR peak detection algorithm are then reapplied to the resampled data.

6.5 ANALYSIS OF EXPERIMENTAL RESULTS

Measurements were performed on the radial artery in the wrist of an healthy human. Typical ECG and MPR signals are

shown in Figure 6.4. Figure 6.5 shows PTT's for fifteen artefact free pulses on two separate days. Unexpectedly, the errors were found to be significantly larger than the theoretical uncertainties (standard deviations of 15.7 ms for day 1, and 9.3 ms for day 2). After careful visual inspection it was apparent that certain pulses appeared to be somewhat distorted compared with other pulses.

An hypothesis was then made that these errors could be attributed to the non-linearity of the MPR device. To investigate this hypothesis a program was implemented on a PDP-11 minicomputer. A template digitized pulse signal, called $z_s(t)$, was normalized to one and was then multiplied by a factor, P. The resulting time-varying signal $Z_{AA}(t) = P(1-Z_n(t))$ simulates an arterial wall motion with peak to peak displacement P and antenna-artery spacing varying from D to P+D. The mathematical representation of the graph in figure 3.4 is given by

$$f(z_{AA}(t)) = A\, e^{-2\alpha Z_{AA}(t)} \sin\left(\frac{2\pi}{\lambda} Z_{AA}(t) + \emptyset\right) \qquad (6.18)$$

Where A = 175.8 mv

α = attenuation in water, 43.6 dB/cm (0.502 np/mm)

λ = wavelength in water, 1.703 mm

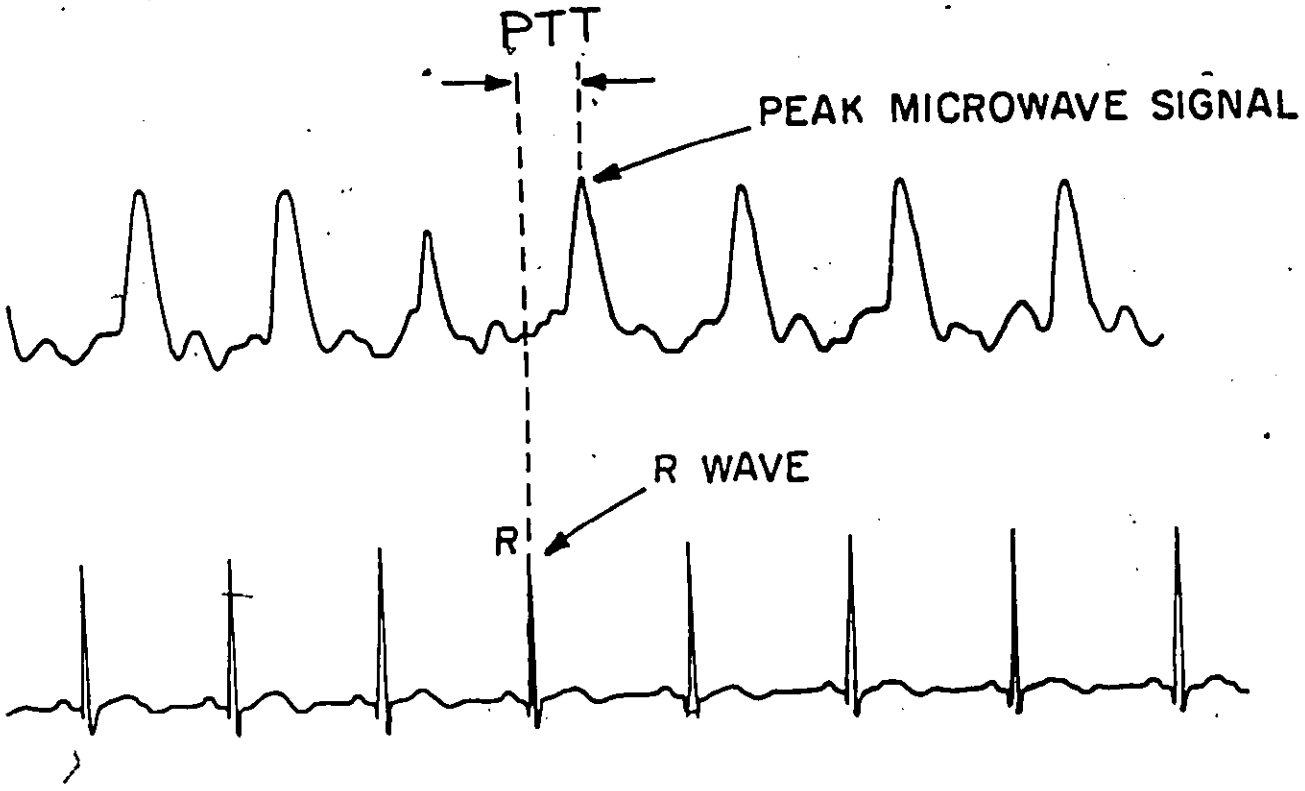

Figure 6.4 Typical timing of ELG R-wave and MPR signal in radial artery.

	DAY 1	DAY 2
TT (ms)	330	330
	302	308
	324	312
	324	325
	325	324
	330	329
	288	332
	332	333
	332	349
	326	326
	359	332
	330	330
	326	328
	325	331
	329	326
MEAN	325	328
S.D.	15.7	9.3

Figure 6.5 Pulse Transit Times (PTT) for fifteen artefact-free Pulses on two separate days.

$\emptyset$ = 2.391 rad.

z = antenna-artery spacing in mm

Therefore the detected Microwave signal corresponding to an arterial wall motion given by $z_{AA}(t)$ is obtained from the above equation. The time of occurence of the peak for $z_{AA}(t)$ and $f(z_{AA}(t))$ were estimated, with the algorithm, for different values of P and D. The probability of making an error due to the distortion of the signal by the detector was estimated by dividing the number of false detections by the total number of trials. This probability was naturally a function of the peak to peak displacement of the arterial wall since the larger the peak displacement the more chances the signal has of being distorted around its peak. The estimated error probabilities are shown in Figure 6:6.

To this date, attempts to obtain calibrated MPR displacement measurements using an interferometer technique have been unsuccessful. It would seem that patient motion, variations in MPR device placement, and variable arterial wall displacement (due to muscular resistance variations for example) causes the MPR to operate in a non-linear portion of its transfer curve occasionally. One way around this problem is to drop PTT measurements which appear to be significantly different than the average, for example those PTT values

which are smaller than the average minus the standard deviation or larger than the average plus the standard deviation. In doing this with the data in Figure 6.5, we obtained means of 328 ms and 329 ms with standard deviations of 3.05 ms and 3.01 ms for the two days.

Measurements were also performed on other arteries of a healthy human. Results of measurements along the aorta and the femoral artery are presented in Figure 6.7. The bars indicate pulse to pulse variability and variations introduced by antenna placement error. From these PTT measurements, the PWV along the arterial segment from the abdominal aorta to the femoral artery is 4.8 mm/ms with an error of 15%.

The main conclusions drawn from this simulation can be summarized as follows:

- PWV measurements with uncertainties lower than 20% difficult to obtain using only one MPR device (would require using a correlation technique and a minicomputer)

- PTT measurements with uncertainties of 2% achievable

- 12 bits/sample for MPR signal and 8 bits/sample for ECG are necessary and 500 sample/sec sufficient for both signals

- resampling to increase peak detection accuracy not advantageous

- necessary to implement a scheme to throw out pulses with PTTs nominally different from a dynamically updated average

- differentiation approach to peak detection sufficiently accurate

- dual microprocessor system necessary

- filtering and peak detection software easily transportable to stand alone microprocessor system

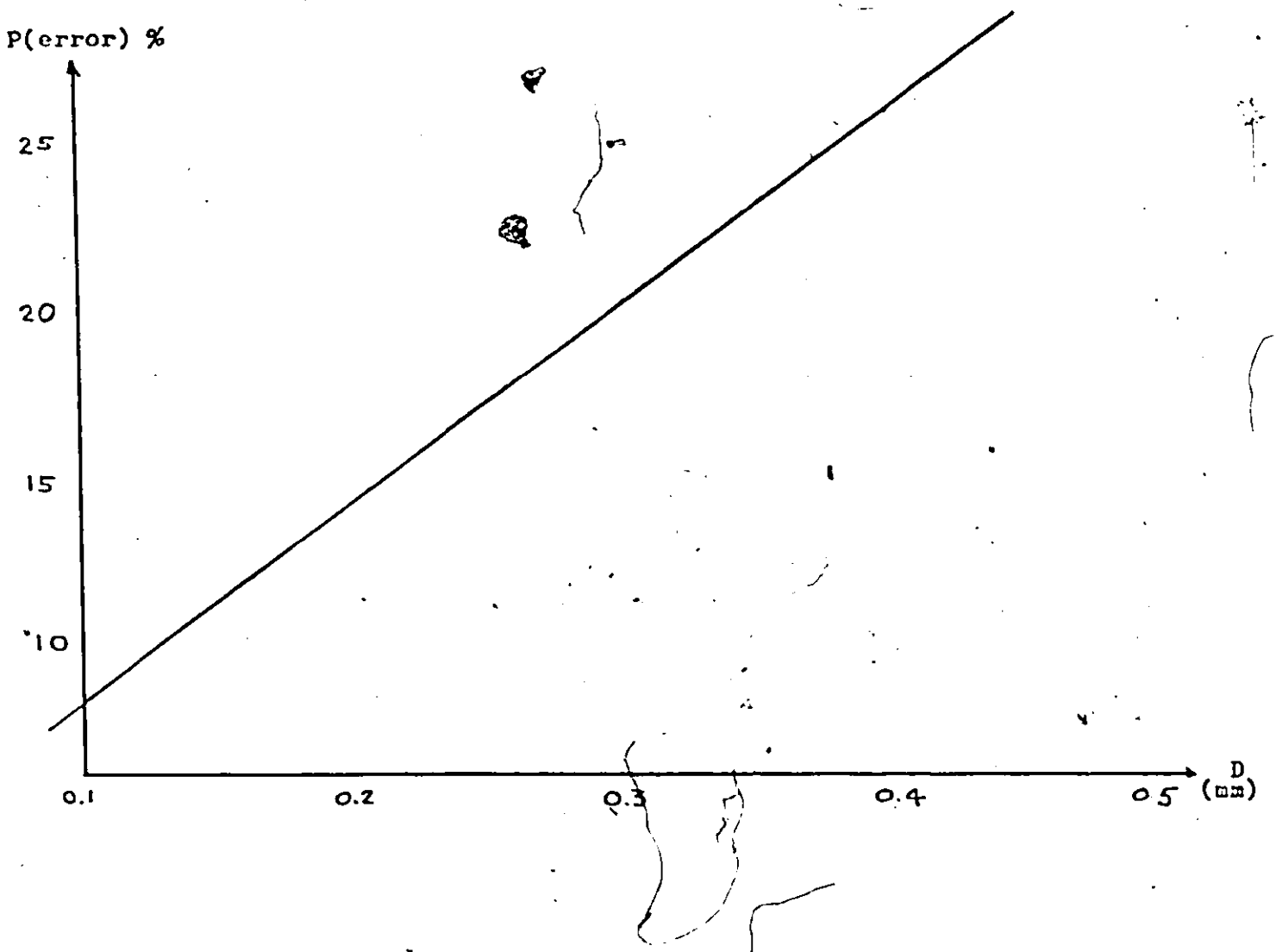

Figure 6.6 Probability of error as a function of peak arterial wall displacement.

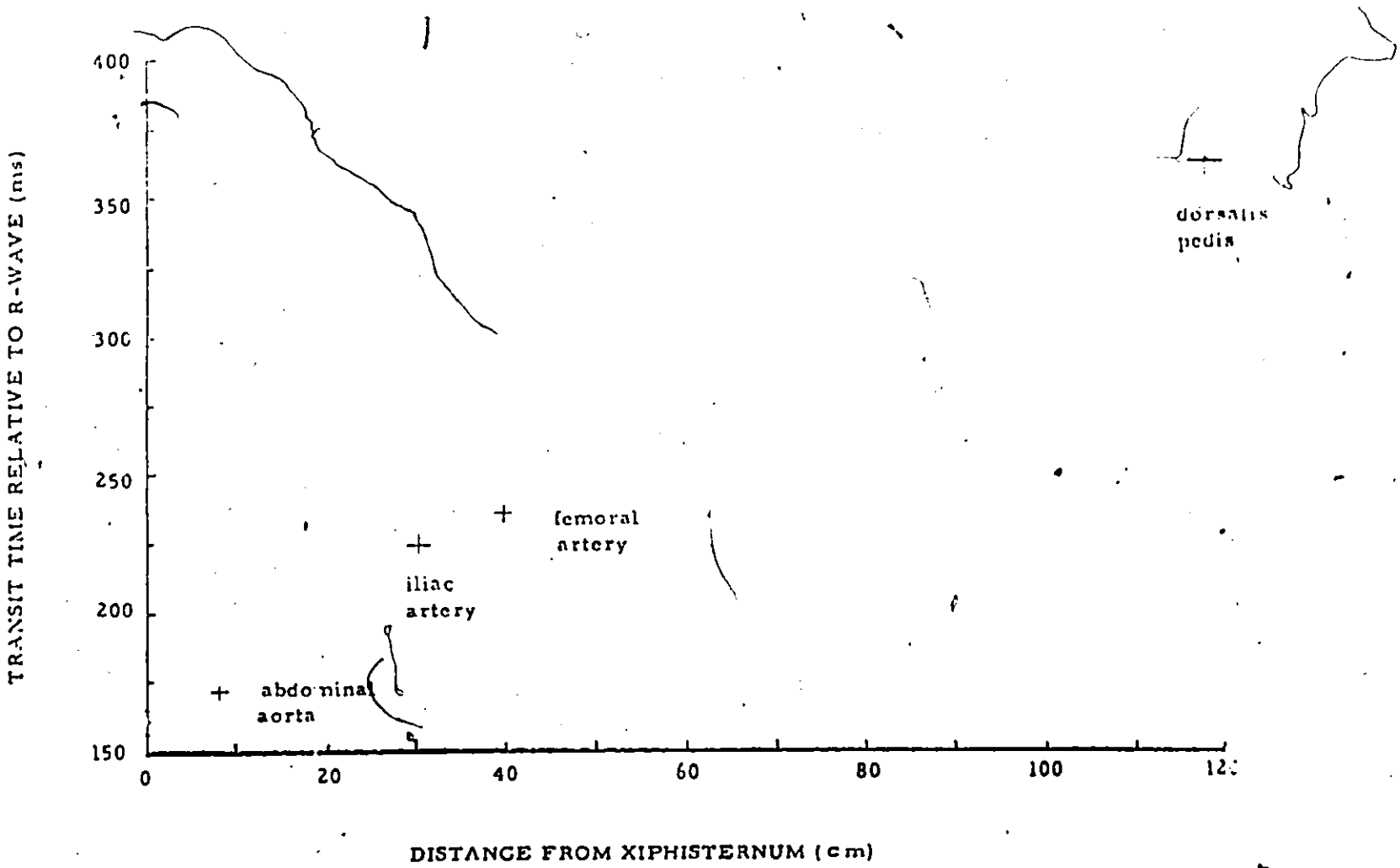

Figure 6.7 Pulse Transit Times (PTT) in aorta, iliae and femoral arteries.

Chapter VII

CARDIOVASCULAR SIGNAL RECORDER GENERAL DESIGN

In the first section of this chapter we will present a general description of the Cardiovascular Signal Recorder (CSR) digital system underlining the motives for the choice of hardware and justifying the system's architecture. Following this we will describe the individual modules comprising the system.

7.1 GENERAL SYSTEM DESCRIPTION

Let use first briefly restate the main tasks that the CSR has to perform, as stated in the previous chapter.

1. Reduce wide band noise generated in the data acquisition module.

2. Artifact detection in the MPR signal.

3. ECG's R-wave detection.

4. MPR signal peak detection.

5. Data acquisition control; such as switching the analog multiplexer, programming the real time clock and reading the ADC.

6. Transfer data to a mass storage unit.

Some of the main criteria taken into account in the CSR system design were portability (size, power consumption), cost, throughput and ease to adapt the system to other cardiovascular monitoring applications. For the reasons stated in chapter 5 a microprocessor based system was considered. The basic components of the system were initially specified to be a microprocessor, an analog to digital converter (ADC), a programmable clock, main memory and mass storage memory.

For several reasons, to be enumerated later, the dual processor unit consists of two microprocessor arranged in a pipeline configuration, communicating via shared random access memory. There are three principal reasons for adopting a shared memory interprocessor communication scheme. First, since the system is relatively small, a "crossbar switching" scheme to switch CPU's and memory modules is simple and does not add excessively to the overall cost of the system. Second, for our particular application, software overhead is minimized. Third, and most important, the main

traffic between the two CPU's consists of data organized or assembled in blocks.

To expand on the third reason it is relevant to discuss a specific CSR task, that of data storage. The main criteria for the selection of the storage unit were: size, cost, power consumption and transfer rates. The Quantex Model 200 mini cassette recorder was chosen. The recording density of the Quantex 200 is 1600 bpi while the maximum transfer rate is 24 kbauds (or 1500 16-bit samples per second). This meets our throughput requirement. To enable the use of the cassette at maximum density independently of the sampling rates, it is necessary to buffer the incoming data from the ADC module. When the buffers are fully loaded they are ready to be dumped on the cassette. The size of the buffer is dictated by a tradeoff between cost of memory and the loss of space on the cassette when it is stoped in between data block transfers. This buffering can be advantageously used as a common memory shared by the two processors. The scheme consists of two RAM blocks which are switched between the two processors. While one processor is filling one memory block with incoming data from the ADC module, the other processor dumps the data onto the digital cassette.

Let us now elaborate on the processing unit. The center of the CSR system consists of two processors pipelined and

arranged in a master and slave configuration. The master processor performs the following functions:

1. Data acquisition control, such as switching the analog multiplexor, programming the real time clock and reading the analog to digital converter (ADC).

2. Data conditioning, such as filtering.

3. Monitoring the activities of the slave processor.

4. Software interface to the peripherals.

The second processor, the slave, performs the bulk of the real time processing.

1. R-wave detection in the ECG.
2. Peak detection in the MPR signal.
3. Calculation of PTT.
4. Transfer data to the digital cassette.
5. Artefact detection in MPR device.

A block diagram of the CSR system is shown in Figure 7.1. The system consists of four basic units; namely, the

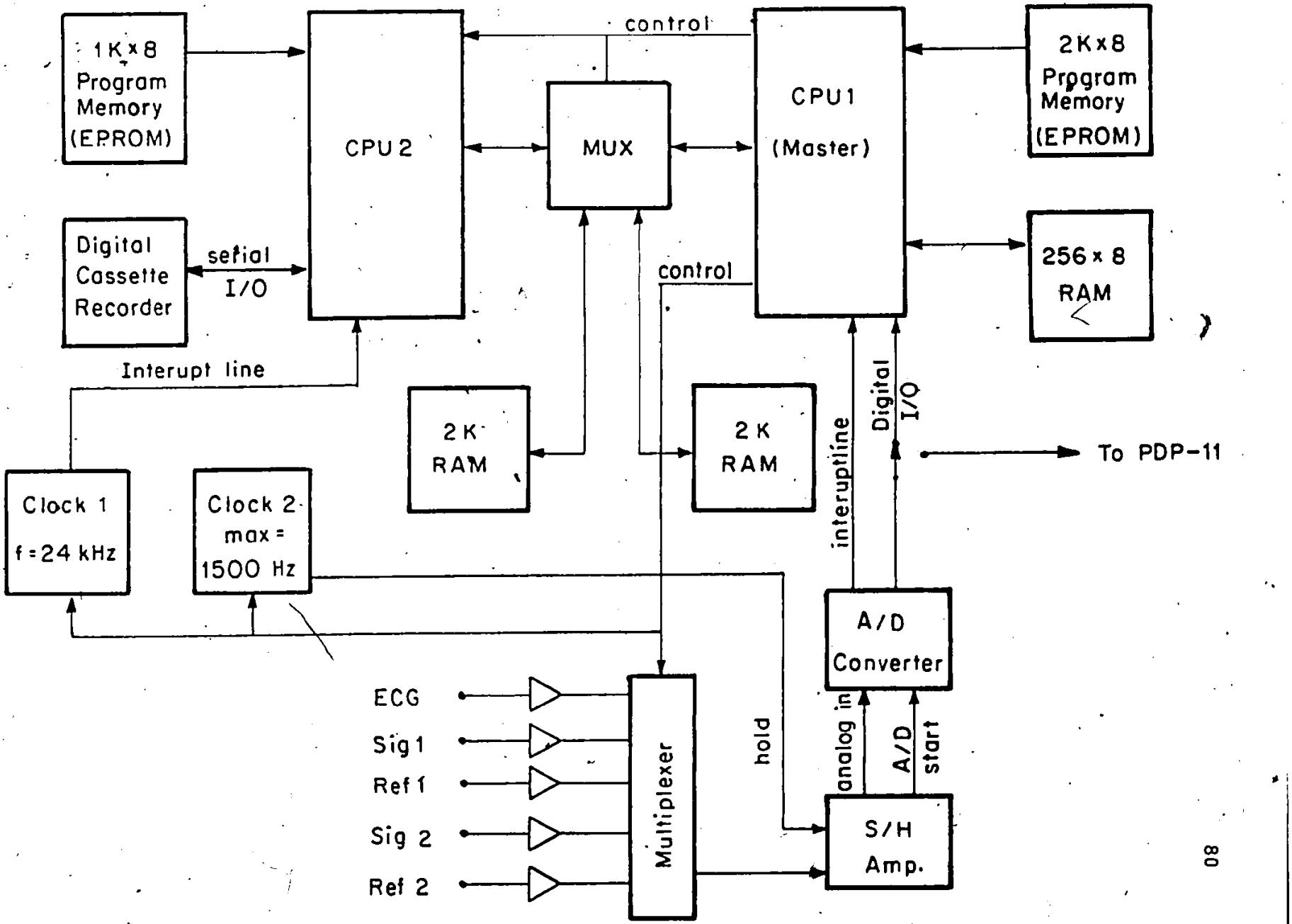

Figure 7. 1 Block diagram of CSR System

processing unit, the data acquisition module, the storage unit and the human interface hardware. In the next section we will describe the processing unit.

7.2 THE CSR PROCESSOR

Recent advances in microprocessor technology have brought into the market powerful 16-bit and 32 bit microprocessors (such as Intel's 8086 and Motorolas MC68000). As expected, however, these microprocessors require higher degrees of development efforts and higher hardware costs than the more tranditional 8-bit machines. Thus, one should carefully evaluate requirements before deciding on a 16 or 32 bit machine. In the case of the CSR system, from the simulation studies in chapter VI the more conventional 8-bit microprocessor was deemed to be of sufficient power to satisfy our requirements.

Since the University of Ottawa department of Electrical Engineering possesses a MDS-800 microprocessor development system, the Intel 8085 microprocessor seemed a good choice for the CPU's. For practical reasons we chose to design the CSR system around a SDK-85 system design kit. The basic SDK-85 has the following built in features: a 3MHz 8085a CPU (1.3 μs instruction cycle), a direct teletypewriter interface, an interactive LED display, a wire wrap area for

customed design circuit, system monitor software in a 2K ROM (8355), 256 bytes RAM, 38 parallel I/O lines (expandable to 76 lines) and a serial I/O thru the SID/SOD ports of the 8085.

In addition to the basic SDK-85 components an 8155 was added, thus providing another 256 bytes of static RAM and an extra 22 programmable I/O lines. Also, expansion buffers were necessary to drive the bus switching controllers, the hardware multiplier and the master processor program memory (a 2K x 8 2716 EPROM). The slave processor is also configured around an 8085 CPU along with an 8155 and a 2716 EPROM, thus providing all I/O lines, data and program memory requirements. The expanded SDK-85 and slave processor circuit diagrams are included in the Appendices.

The program which supervises and coordinates all activities of the CSR is called SUPCSR. SUPCSR starts to run as soon as the CSR system is turned on. It initially acquires from the user all information and parameters necessary for a recording session. When the data acquisition process is initiated by the user, SUPCSR is responsible for handling software interrupts (such as overflows, inter-processor communication synchronization errors, status errors, etc....) generated by the application software as

well as managing system operations such as monitoring the data acquisition and coordinating the activities of the slave processor.

Interaction of SUPCSR with application programs and peripherals devices will be further discussed in the following sections.

7.3 MEMORY SHARING AND INTERPROCESSOR COMMUNICATION

As mentioned earlier, the two processor can access common data through shared RAM. Two blocks of RAM are alternately switched between the two processors. This scheme is particularly desirable for our application since the two processors are pipelined and the transfers between them are in blocks of data. This eliminates contention for resources among the processors and minimizes the effect of the multiprocessing law of diminishing marginal utility, [39]. Also, software overhead is minimized since there is no complex scheduling.

The memory processor bus switches (or bus multiplexer) consists of bidirectional drivers with tri-state outputs. The master processor controls the output state of the drivers in such a manner that when it accesses a block of memory the other processors bus is branched to the other block. The

read signal from each processor controls the direction of the drivers to which they are connected.

In order to establish a rule for the selection of the size of the memory blocks it is necessary to digress from the current discussion to talk about the cassette recorder subsystem. As previously mentioned, the shared memory inter-processor communication scheme was considered mainly because it is necessary to buffer the data anyway. This arises because the cassette recorder servo drives the cassette at a constant read/write speed of 15 ips. Since the cassette recording density is 1600 bpi, the maximum transfer rate to the cassette is 24 kbauds (i.e. 1500 16-bit words per second). Thus, in order to be able to use the cassette at maximum density, independantly of the sampling rates, it is necessary to buffer the incoming data from the A/D module and transfer it to the cassette at maximum speed, stoping the cassette drive between the data block dumps.

Given that the start/stop time of the cassette drive is 30 ms and that the cassette capacity is C words we can relate the size of the RAM blocks, say X 16-bit words, to the fraction of the total cassette capacity that we want to use, say Y %. For each block dumps we lose the equivalent of 60 ms of cassette space for start and stop, which is equivalent to 90 words (i.e. 1500 x 0.06). The total number of words

that will be stored on a cassette is therefore C - (90C/X). We therefore have C - (90C/X) = YC/100,or X=90/(1-Y/100). Therefore, if we wish to use 90 % of the total cassette capacity the RAM block size is 900 words. Two blocks of 2K x 8 RAM's were therefore chosen as the buffer area. The MOSTEK 4118's were found to have sufficient bandwidth (120 ns) and feature a latch function which permits the latching of the address for time multiplexed buses.

The bus switches consists of eight 8286 bidirectional bus drivers with tri-state outputs. The master processor, controls the output data of the drivers. Immediately after switching the RAM blocks, SUPCSR (master CPU) requests the services of the slave processor by sending it an interrrupt through an I/O line. The nature of the services (or processing requirements) is coded into the first word of each memory block and is called the request status word (RSW). The slave processor returns a processing status word (PSW) in the second word of the memory block. The PSW is monitored by SUPCSR which verifies the proper operation of the slave activities and takes action if required.

7.4 THE ADC MODULE

The data acquisition unit consists of an 8-channel analog multiplexer, a sample and hold amplifier (SHA), a

12-bit analog to digital coverter (ADC) and an 8253 programmable interval timer (PIT). The PIT is organized as three independant counters which can be programmed by a microprocessor as divide-by-N counters. One timer is used as a rate generator for the SHA. Another timer supplies the digital cassette transfer rate. The end-of-conversion (STS) signal of the ADC is used to interrupt the master processor. At that point SUPCSR takes over and fetches the 12-bit result through an I/O port. The total acquisition time, including hardware and software delays is approximately 147 us per sample which corresponds to a maximum overall sampling rate of 6800 samples per second.

At the beginning of a session the user is asked to specify how many analog channels are to be sampled as well as the required sampling rate. SUPCSR then calculates the required count and loads it into one of the programmable clock counters through an I/O. A nominal clock counting rate of 1.5 MHz is taken from the master processor's clock (through a divide-by-two counter). The count required for the cassette transfer rate is also automatically loaded into a second counter.

The analog multiplexer is an Analog Devices AD7501. The address for selecting one of eight input analog channels is supplied by a 4-bit I/O port on the master processor. At

system initialization, all components of the A/D module are disabled. When the user has specified all parameters required for a recording/processing session and is ready to start the process, he presses the start acquisition button. This starts up the counters on the PIT. The clock output of the first counter then goes through a monostable multivibrator which supplies a 400 ns negative pulse for the start-conversion signal on the ADC. Upon completion of the first A/D conversion, the ADC's STS signal generates an 800 ns positive pulse (again through a monostable multivibrator) which is used to interupt the master processor on RST 6.5. SUPCSR then enables the analog multiplexer with the first channel selected. The STS signal from the ADC is also used as a sample and hold signal to the SHA.

7.5 DIGITAL CASSETTE RECORDER SUBSYSTEM

We have already discussed several aspects of the digital cassette recorder in detail in the previous sections. In this section we will consider cassette handling aspects. As mentioned earlier the slave processor is responsible for transfering data to the digital cassette. The slave processor starts transfering a data block when SUPCSR informs it to do so. However, before data can be transfered to the digital cassette, the slave processor has to start the

servo/data writing circuits. These controls are performed through two I/O ports.

The transfer rate is supplied by a clock which interrupts the slave processor on RST 7.5. The interrupt service routine simply puts the next bit to be transfered on the SOD (serial output). That bit is then transfered to the cassette on the next clock pulse. In between each interrupt the application software performs the required data processing as well as supervising the transfering status, that is it makes sure that the processing rate is faster than transfering rate, keeps track of the next word and bit to be transfered and stops transfering data at the end of the blocks. At the end of a block dump the cassette drive is stopped and the servo/data writing circuits are disabled.

In addition to the above cassette handling operations the slave processor is also responsible for rewinding and reading the data. This is required to either perform off-line processing or to send the data to a PDP-11 microcomputer. Mechanisms for transfering data to the PDP-11 were considered for the following reasons:

1. For more complex off-line processing.
2. For computation of inter-patient statistics.
3. To archive recordings on disk or magnetic tape.

The data transfer is interrupt driven and coordinated by the PDP-11 which directs the CSR to transfer the data through I/O ports.

7.6 THE HARDWARE MULTIPLIER

The necessity for a hardware multiplier was clear after the CSR simulation (Chapter 6). A typical hardware multiplier such as the Monolithic Memory 67558 performs an 8 x 8 bit multiplication in 100 ns. The factor limiting the multiplication speed is therefore the time required to output and input the arguments and result. For a 16 x 16 bit multiplication we have the following equation:

$$X_{0-15}\,Y_{0-15} = (X_{0-7}\,Y_{0-7} + 2\,\lceil(X_{0-7}\,Y_{8-15}) + X_{8-15}\,Y_{0-7})\rceil + 2\,(X_{8-15}\,Y_{8-15}) \qquad (7.1)$$

Thus we must perform four 8 x 8 bit multiplication. If I/O ports are used to transfer data to/from the multiplier eight output and eight input operations are required. With an 8085 microprocessor this represents about 53 µs without including overhead for addition and getting operands from the memory. For a 2nd order filter this implies 5 multiplications x 53 µs = 267 µs per sample. At a 1000 Hz sampling rate this means that the CPU would spend about 27% of its time for filtering, which is unacceptable for the CSR.

Master [private communication] described a method in which external instruction execution hardware, such as a multiplier, is connected in such a way that it is transparent to the programmer. This method permits to reduce the relative time spent for filtering to around 10%. With Master's method an instruction of the 8085 is detected by hardware which activates the hardware multiplier. In our case the instruction dedicated as a "multiply instruction" is MOV H,M. Here the multiplicand and multiplier are stored in registered H and L. During the opcode fetch cycle of the MOV H,M instruction, the special hardware detects the opcode. The external circuit then disables the RD signal to the rest of the CSR and enables the multiplier. On the next clock cycle the H and L contents are sent on the address bus which is connected to the input of the multiplier. The result appears on the data bus 100 ns later and is picked up and loaded into the H register by the CPU. For a 16 x 16 bit multiplication this requires 18 μs. This method is therefore very efficient since there is an increase of almost 300 % in speed over the I/O method. However, there is the expense of losing the original function of the dedicated instruction, MOV H,M.

In this chapter we have presented a description of the CSR digital system. The detailed circuit diagrams are shown in Appendix A.

Chapter VIII

CONCLUSIONS

A microprocessor based system for the analysis of arterial pulse pressure signals obtained from a microwave pulse recorder (MPR) was designed. This system, referred to as the cardiovascular signal recorder (CSR) was intended primarily as a research tool for clinically measuring characteristics of the arterial pulse pressure wave as obtained with the MPR device.

A review of current literature revealed that the pulse wave velocity (PWV) and the pulse transit times (PTT) obtained from arterial pulse waves correlated with several hemodynamic and cardiovascular parameters such as arterial transmural pressure, arterial system anatomy and mechanical properties such as arterial wall elasticity and endocrine disorders. Literature also indicated that arterial pulse waves were obtained either invasively using intra-vascular pressure transducers or non-invasively using ultrasound transducers to measure arterial wall displacements. Both these techniques were shown to have limitations. Invasive transducers are surgically inserted in arteries which limit their use to cases where the invasion of the blood vessels

is justified by the condition of the patient. Ultrasound transducers have limited range in biological tissues and are therefore limited to the measurement of peripheral arteries. The MPR was found to be capable of monitoring, non-invasively, arterial wall motion. Because of the high penetration depth of microwave energy in biological tissues, deeply situated arteries such as the aorta and iliac arteries, can be monitored.

The CSR was designed around a microprocessor based system because of the many benefits including reduced system volume hence portability, reduced power consumption, smaller number of interconnects hence increased reliability, and system programmability resulting in a simplified design and flexibility. Relevant digital processing techniques and hardware available for building microprocessor based systems were evaluated. A prototype simulation CSR system was then implemented using a microcomputer development system.

The measurement technique used to obtain the PWV and PTT involved detecting the R-wave location in the Electrocardiogram and the peak MPR signal. Since only one MPR device was available, measuring the PWV required measuring the PTTs at two locations along an artery segment and taking the difference of the two. An uncertainty analysis suggested that it was possible to reduce the uncertainty on the PTT

measurement to under 1.2 msec and consequently that of the PWV measurement to 15% by resampling the ECG and MPR signals originally sampled at 500 samples/sec. It was also assumed that meaningful physiological variability of PWVs was larger than 15%.

The simulation CSR system consisted of an MDS800 microcomputer development system, a 16-channel analog multiplexer, a 12 bit analog to digital converter, a storage scope and two floppy disk drives. Signal processing algorithms for data filtering, ECG R-wave and peak MPR signal detection were implemented and coded to run on the MDS800's 8080 microprocessor. Since the 8080 microprocessor is relatively slow, the processing algorithms could not handle real-time beat to beat PTT measurements. It was therefore determined that the CSR system would be based on a dual 8085 microprocessor system along with a hardware multiplier to perform filtering and data resampling. Since the 8085's instruction set is a superset of that of the 8080's it would be easy to implement the processing algorithms on the 8085 processors.

Experimental results obtained with the simulation system showed that the uncertainty on the PTT measurements were much larger than predicted. Further analysis on a PDP 11 minicomputer revealed that the non-linear behaviour of the

MPR device distorted the actual arterial wall displacement information to a degree proportional to the MPR antenna to arterial wall distance, thus resulting in false peak detection. It was hypothesized that the arterial wall to antenna distance could change fractionally during a measurement session causing the MPR device to operate in an highly non-linear region of its transfer curve. This could be caused by patient body motion, muscle activity in the area of the monitored artery or by MPR device movement caused by inadequate fixing of the device to the patients body. A scheme was devised to overcome that problem by throwing out pulses with measured PTTs grossly different from a dynamically updated running average. When implementing this scheme the experimental uncertainties were considerably reduced. The remaining observed discrepancy between experimental and theoretical uncertainties can be attributed to a number of factors including arterial pulse wave reflections in the arterial tree resulting in distorted arterial wall displacements and actual real variations due to hemodynamics changes.

Nevertheless, the simulation CSR system demonstrated the feasibility of the CSR system. It showed that the resampling process to increase peak detection accuracy was not required since observed uncertainties were larger than theoretically achievable without the resampling. From the simulation it

was therefore possible to specify the CSR design goals and parameters. The complete CSR system was then designed and specified to achieve those requirements. It was however beyond the scope of this thesis to implement the CSR system. This would constitute an interesting undergraduate project.

9.0 REFERENCES

1. Stuchly, S.S., Smith, A., Goldberg, M., Thansandote, A. and Ménard, A. (1980), "A Microwave Device for Arterial Wall Motion Analysis", 33rd ACEMB' Washington, D.C., p.57.

2. Ganong, W.F., (1973), Review of Medical Physiology, Lange Medical Publications, Los Altos California.

3. McDonald, D.A., (1968), "Regional Pulse Wave Velocity in the Arterial Tree", Journal of Applied Physiology, Vol. 24, No. 1.

4. Newman, D.L. and Grennwald, S.E., (1978), "Validity of the Moens-Korteweg Equation", The Arterial System, R.D. Bauer and R. Busse editors, Springer Verlag, Berlin, pp. 109-115.

5. Bergel, D.H., (1978), "Mechanics of the Arterial Wall in Health and Disease", The Arterial System, R.D. Bauer and R. Busse editors, Springer Verlag, Berlin, pp. 3-14.

6. Westerhof, G.C., Bos, V.D. and Laxmina, S., (1978), "Arterial Reflection", The Arterial System, R.D. Bauer and R. Busse editors, Springer Verlag, Berlin, pp. 48-62.

7. Wetterer, E., Bauer, R.D. and Busse, R., (1978), "New Ways in Determining the Propagation Coefficient and the Visco-Elastic Behaviour of Arteries in Situ", The Arterial System, R.D. Bauer and R. Busse editors, Springer Verlag, Berlin, pp. 35-47.

8. Kemmer, T., (1978), "Models of the Arterial System", The Arterial System, R.D. Bauer and R. Busse editors, Springer Berlag, Berlin, pp. 80-88.

9. Oddou, C., Flaud, P. and Geiger, D., (1978), "Model of Non-Linear Viscoelastic Wall Rheology Applied to Arterial Dynamics", The Arterial System, R.D. Bauer and R. Busse editors, Springer Verlag, Berlin, pp. 101-108.

10. Clark, J.W., Ling, R.Y.S., Srinivasan, R., Cole, J.S. and Pruett, R.C., (1980), "A Two Stage Identification Scheme for the Determination of the Parameters of a Model of the Left Heart and Systemic Circulation", IEEE trans. on Biomed. En., Vol. 13, No. 1, JAN, pp. 20-29.

11. Gribbin, B., Steptoe, A. and Sleight, P. (1976), "Pulse Wave Velocity and Blood Pressure Change", Psycho-physiology, Vol. 13, No. 1, pp. 86-90.

12. Steptoe, A. Smulyan, H. and Gribbin, B. (1976), "Pulse Wave Velocity and Blood Pressure Change: Calibration and Applications", Psychophysiology, Vol. 13, No. 5, pp. 488-493.

13. Delta Corte, M., Locchi, F., Spinelli, E. and Scarpelli, P.T. (1979), "Effect of the Anatomical Structure of the Arterial Tree on the Measurement of Pulse Wave Velocity in Man", Phys. Biol., Vol. 24, No. 3, pp. 593-599.

14. McDonald, D.A. (1968), "Regional Pulse Wave Velocity in the Arterial Tree", Journal of Applied Physiology, Vol. 24, No. 1.

15. Young, R.T., Van Herle, A.J. and Rodbard, D. (1976), "Improved Diagnosis and Management of Hyper-and Hypothyroidism by Timing of Arterial Sounds", J. Clin. En-docrinol. Metab., Vol. 42.

16. Braver, F.S. and Butler, L.A. (1977), "Cardiovascular Monitoring via Arterial Pulse Wave Training", Med. Electronics, Sept.-Oct., pp. 39-41.

17. Wallace, J.D. and Cade, C.M. (1974), "Clinical Thermography", Crit. Rev. Bioeng., Vol. 2, pp. 39-94.

18. Mills, C. (1977), "The Electromagnetic Flowmeter", Medical Instrumentation, Vol. 11, No. 3, pp. 136-138.

19. Duncan, G.W., Gruber, J.O., Dewey, C.F., Myers, G.S. and Lees, R.S. (1975), "Evaluation of Carotid Stenosis by Angiography", New England Journal of Medecine, Vol. 293, No. 22.

20. Sidgell, J. (1975), "Venous Occlusion Pletysmography", Biomed. Eng., Aug. pp. 300-302 and Sept. pp. 342-349.

21. Gosling, R.G., King, D.H., Newman, D.L. and Woodcock, J.P. (1963), "Transcutaneous Measurement of Arterial Blood Velocity by Ultrasound", Journal of Ultrasonics, pp. 16-23.

22. Barnes, R.W. and Garrett, W.V. (1978), "Intraoperative Assessment of Arterial Reconstruction by Doppler Ultrasound", Surg., Gynecol., and Obst., Vol. 146, June, pp. 896,900.

23. Bushman, W. (1973), "Ultrasonic Imaging of Arterial Wall Echoes", Ultrasound in Med. and Biol., Vol. 1, pp. 33-43.

24. Olsen, C.F. (1977), "Doppler Ultrasound: A Technique for Obtaining Arterial Wall Motion Parameters", IEEE trans. On Sonics an Ultrasonics, Vol. SU-24, No. 6, Nov. pp. 354-358.

25. Thansandote, A. (1981), "Monitoring Time-Varying Biological Impedances at Microwave Frequencies", Ph.D. Thesis, Carleton University.

26. Lim, J.C., (1978), "Microwave Biophysics", Microwave Bioeffects and Radiation Safety, Trans. Inter. Microwave Power Inst., Vol.8, pp.15-54.

27. Stearns, S. D., (1975), Digital Signal Analysis, Hayden Book Co., Rochelle Park, New Jersey.

28. Benson, A.S. (1976), "Bandwidth, Sampling, and Quantizing for Automated ECG Processing", Computers in Cardiology, Oct. 7-9, pp. 295-302.

29. Cox, J.R., Nolle, F.M., Arthur, R.M. (1972), "Digital Analysis of the Electroencephalogram, The Blood Pressure Wave, and the Electrocardiogram", Proc. IEEE, Oct., pp. 405-432.

30. Webster, J.G., (1978), Medical Instrumentation, Houghton Milflin Co., Boston.

31. Harris, F.J., (1978), "On the Use of Windows for Harmonic Analysis with Discrete Fourier Transform", Proc. IEEE, Vol. 66, No. 1, Jan., pp. 51-83.

32. Nutall, A.H. (1981), "Some Windows with Very Good Sidelobe Behaviour", trans. on Accoustics, Speech, and Signal Processing, Vol. ASSP-29, No. 1, Feb., pp. 84-90.

33. Taub, H. and Schilling, .L. (1971), Principles of Communications Systems, McGraw Hill, New York.

34. Crochiere, R.E., and Rabiner, L.R. (1979), "A Program for Multistage Decimation, Interpolation and Narrowband Filtering", Programs for Digital Signal Processing, IEEE Press, New York, pp. 8.3-1 - 8.3-14.

35. Petersen, D.P. and Middleton, D., (1962), "Sampling and Reconstruction of Wave Number Limited Functions in N-Dimensional Eudidean Spaces", Information and control 5, pp. 279-323.

36. Forgues, P.M. and Goldberg, M., (1979), "Microprocessors in Biomedical Instrumentation", IEEE trans. on Instr. and Meas., Vol. IM-28, No. 4, Dec. pp. 250-253.

37. Shackll, A.F., (1981), "Microprocessors and the M.D.", IEEE Spectrum, April, pp. 45-49.

38. Klig, V., (1978), "Biomedical Applications of Microprocessors", Proc. of the IEEE, Vol. 66, No. 2, Feb., pp. 151-161.

39. Fuller, S.H., Ousterhout, J.K., Raskin, L., Rubinfeld, P.I., Sindhu, P.J. and Swan, R.J., (1978), "Multi-Microprocessors: An Overview and Working Example", Proc. IEEE, Vol. 66, No. 2, Feb., pp. 216-228.

40. Satyanarayanan, M., (1980), "Commercial Multiprocessing Systems", IEEE Computer, May, pp. 75-96.

41. Covvey, H.D. and McAlister, N.H., (1979), "Computers in the Practice of Medecine", IEEE/EMBS Newsletter, Vol. 18, No. 2, June, pp. 14-17.

APPENDIX

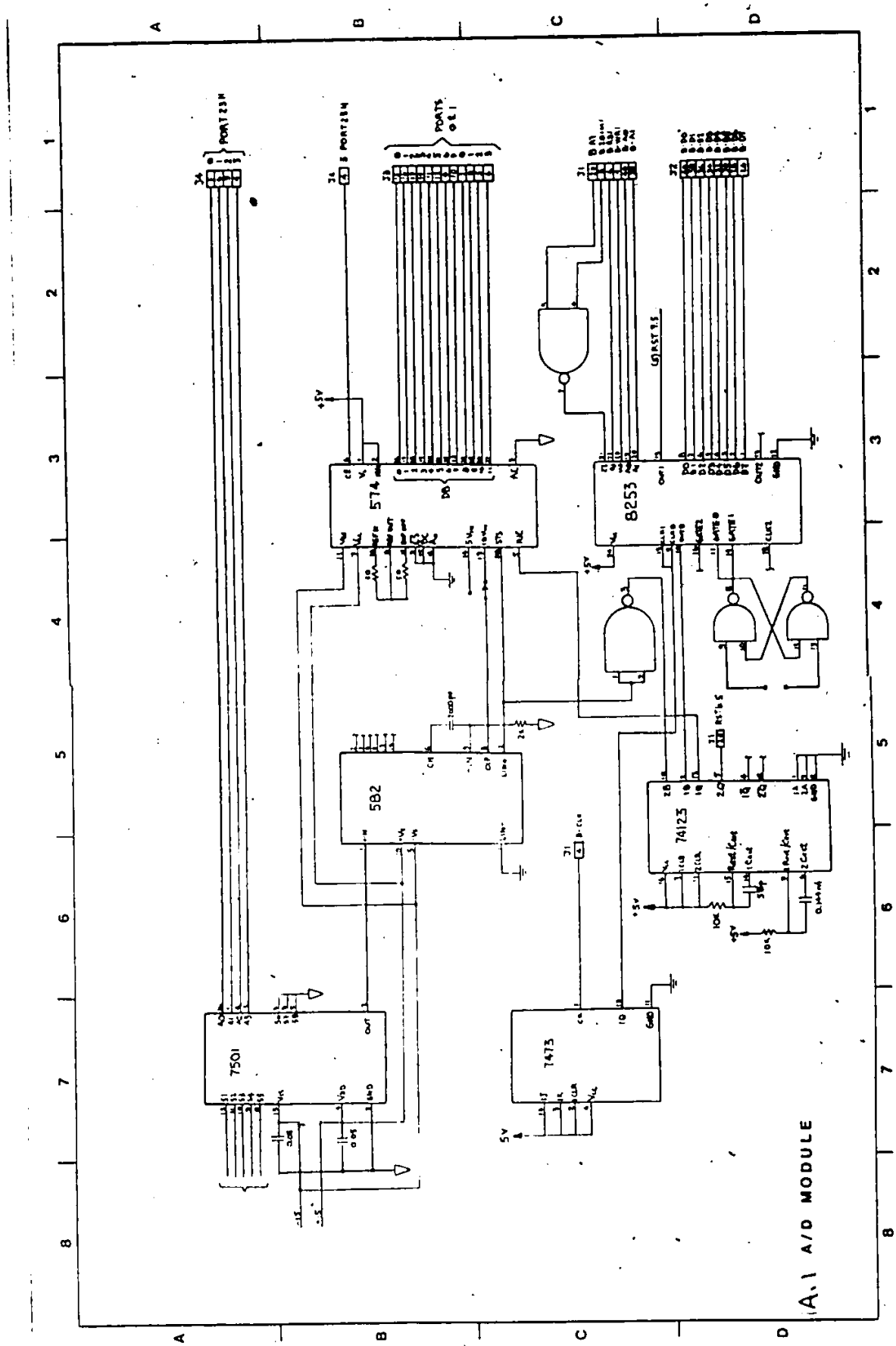
574
8253
582
74123
7501
7473
A.1 A/D MODULE

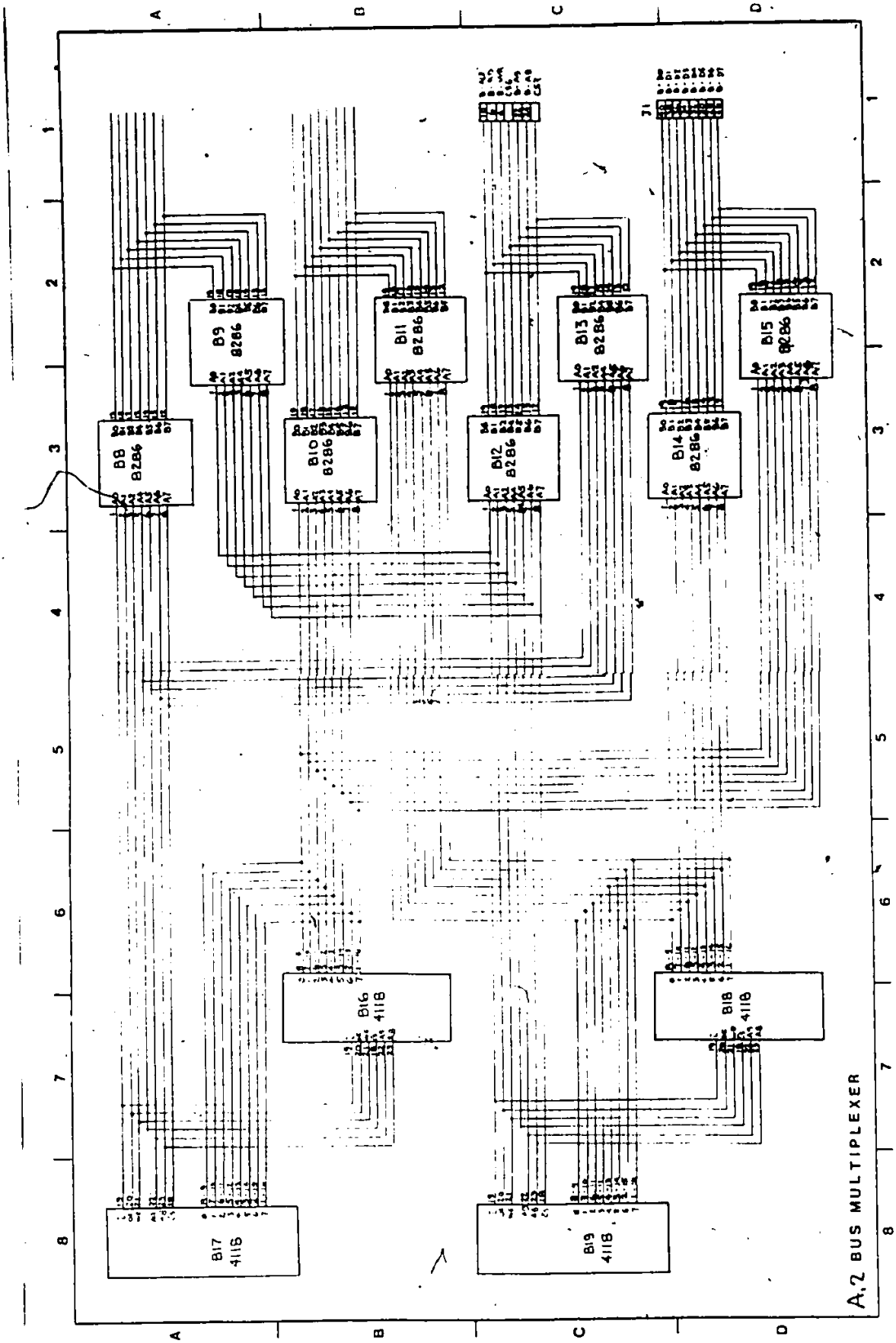
A
B
C
D
1
2
3
4
5
6
7
8
B8 8286
B9 8286
B10 8286
B11 8286
B12 8286
B13 8286
B14 8286
B15 8286
B16 4118
B17 4118
B18 4118
B19 4118
A,2 BUS MULTIPLEXER

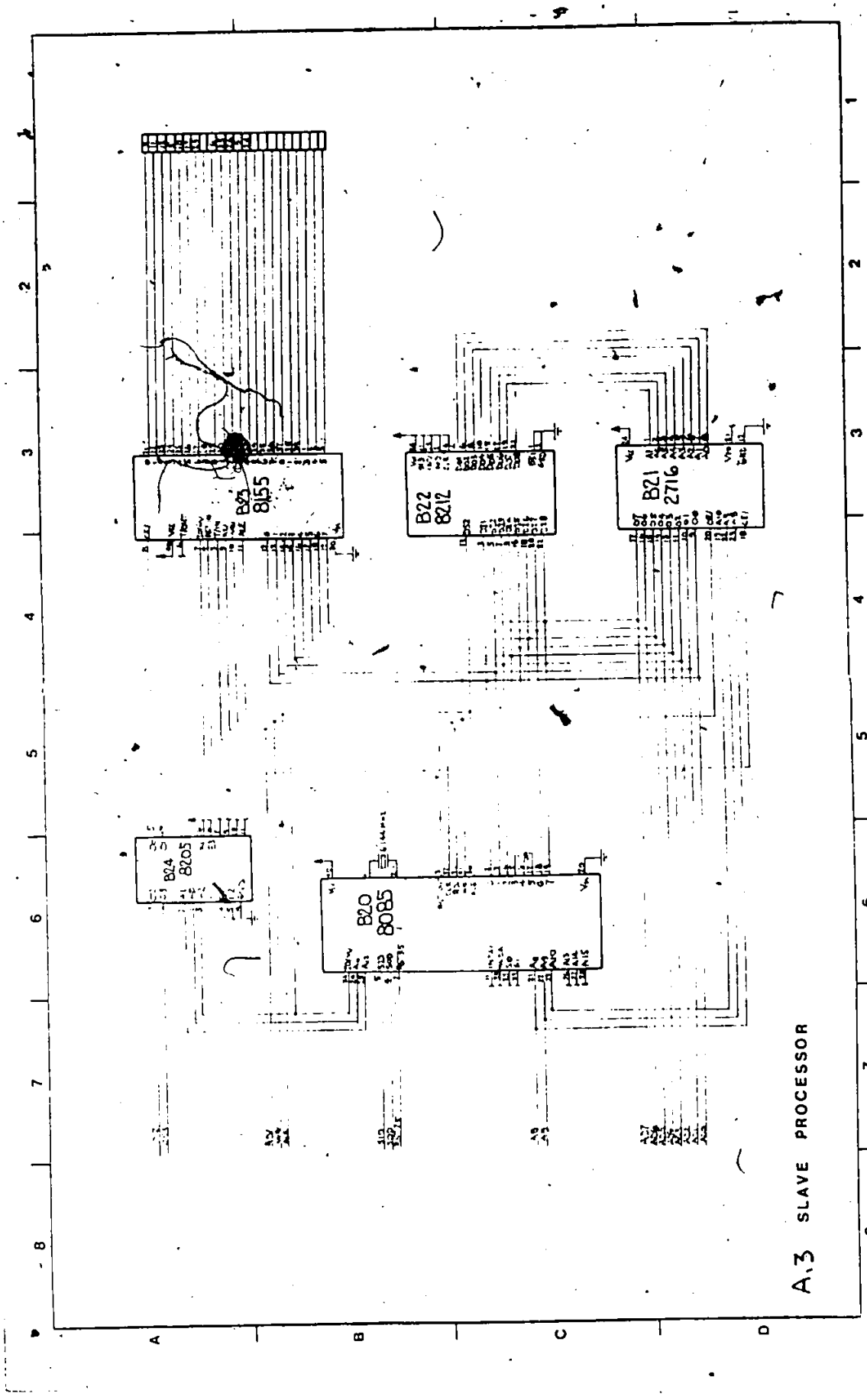
B23
8155
B22
8212
B21
2716
B24
8205
B20
8085
A,3 SLAVE PROCESSOR

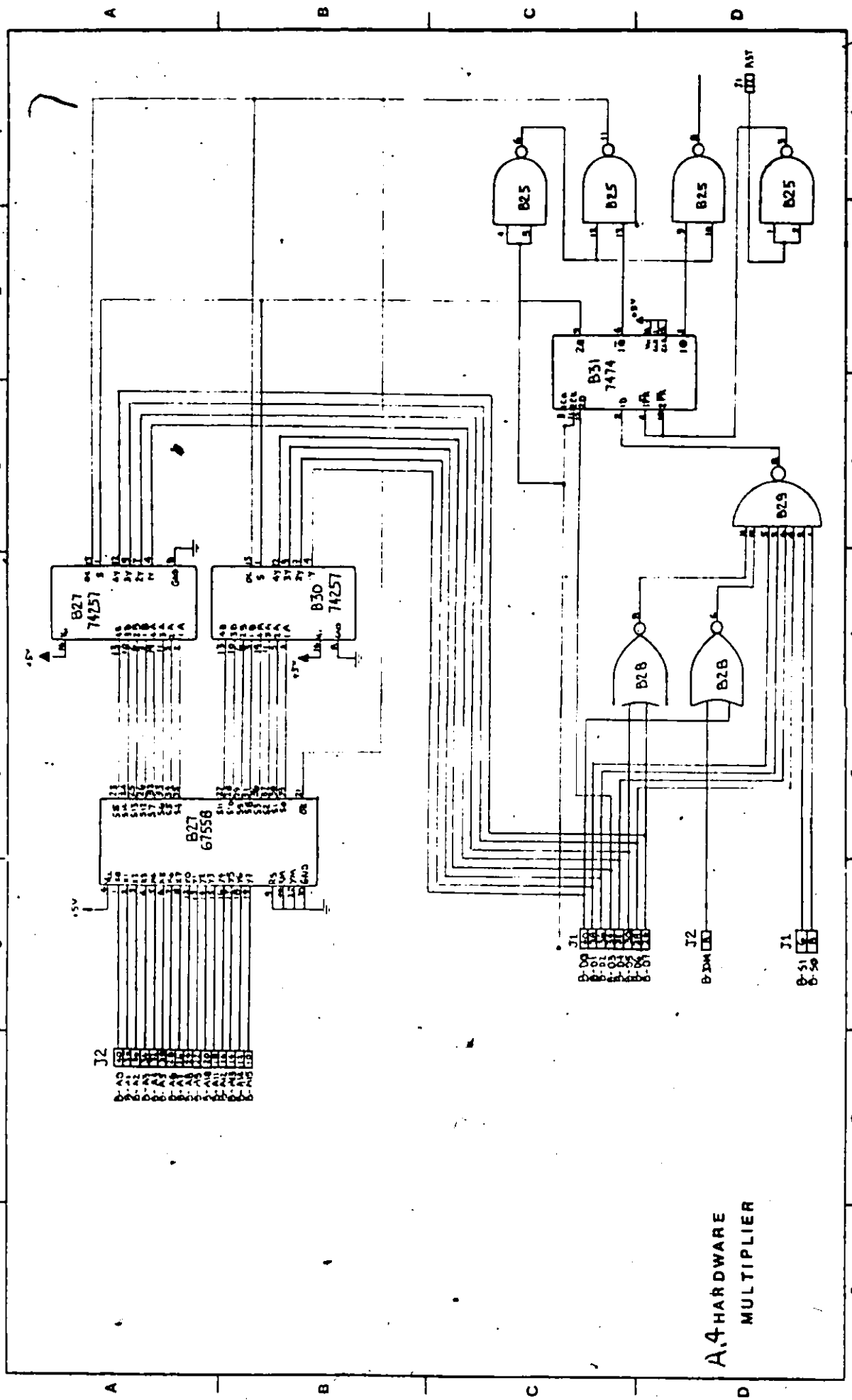
A,4 HARDWARE MULTIPLIER
B25
B31 7474
B29
B28
B27 74257
B30 74257
B27 67558
J1
J2

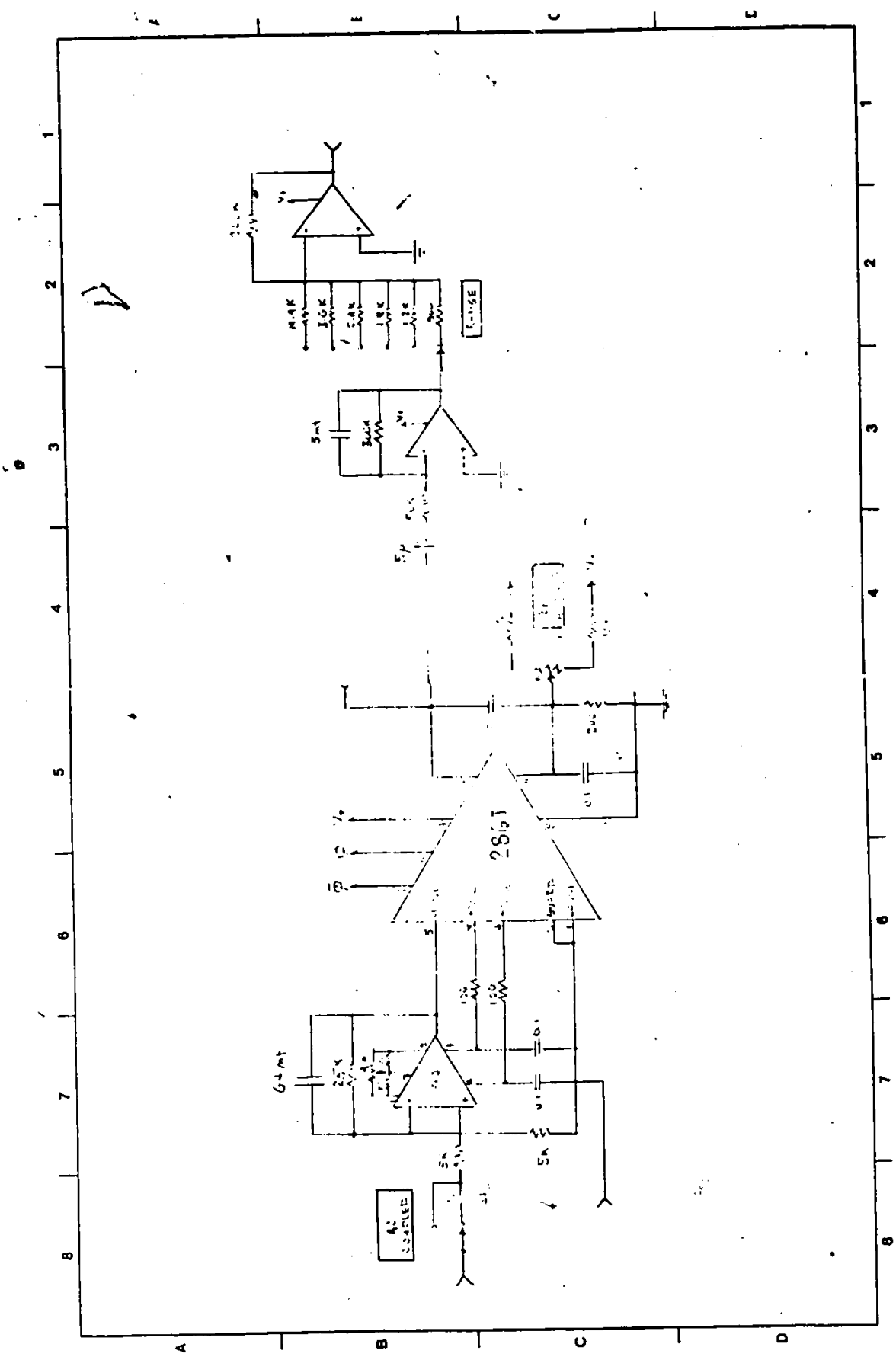

A.5 MPR amplifier circuit diagram

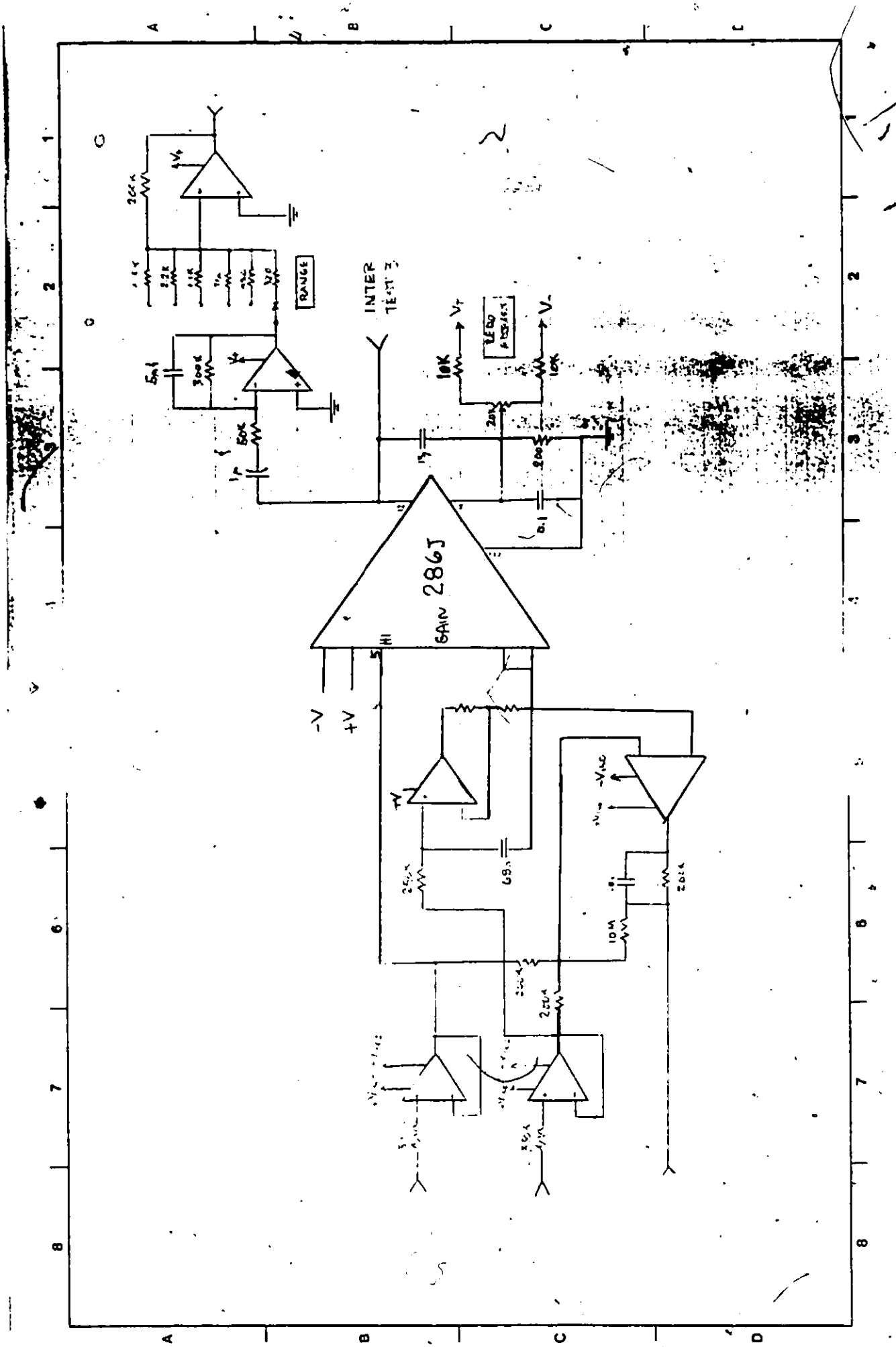

A.6 Electrocardiograph circuit diagram

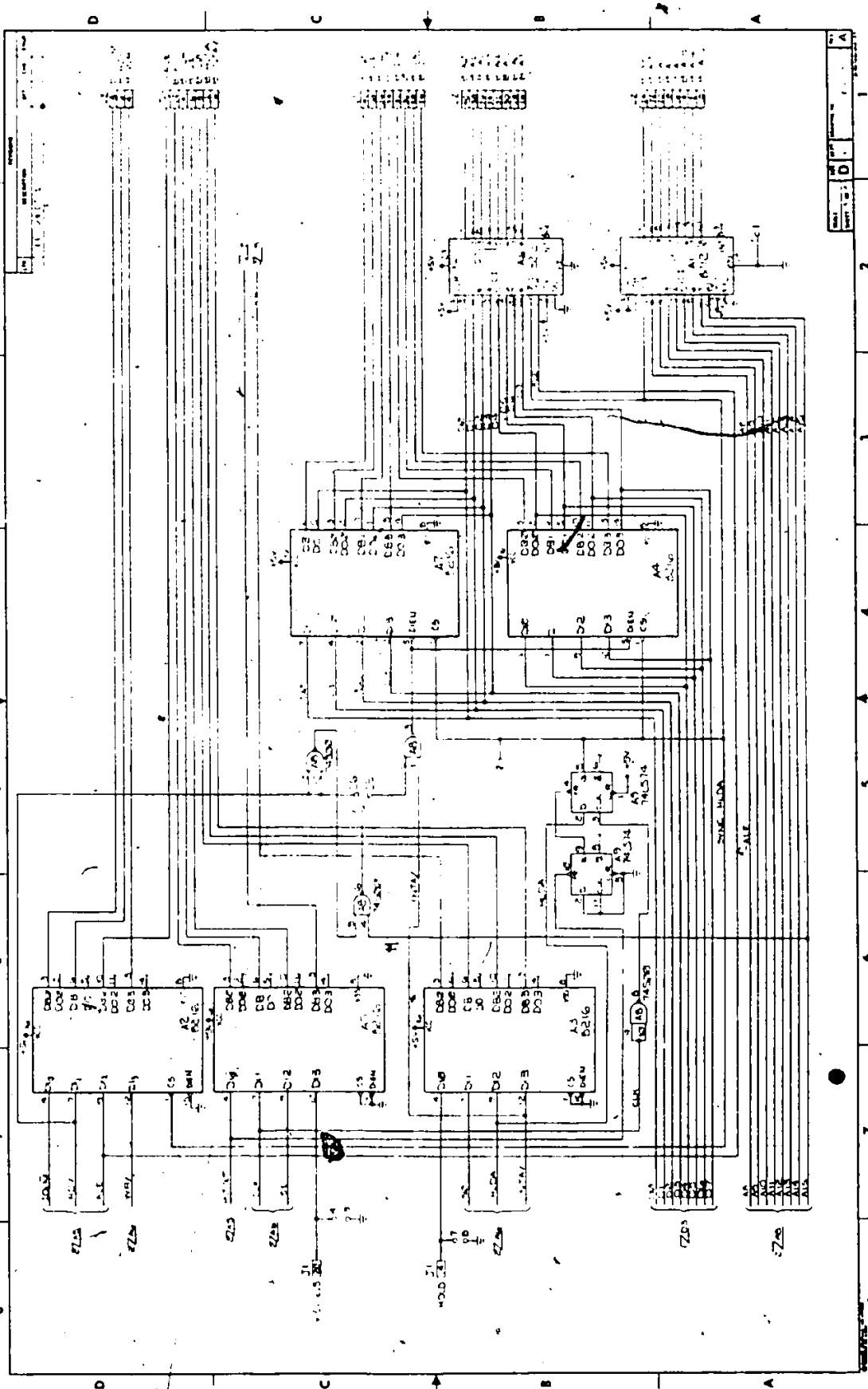

A.7 SDK85 circuit diagram

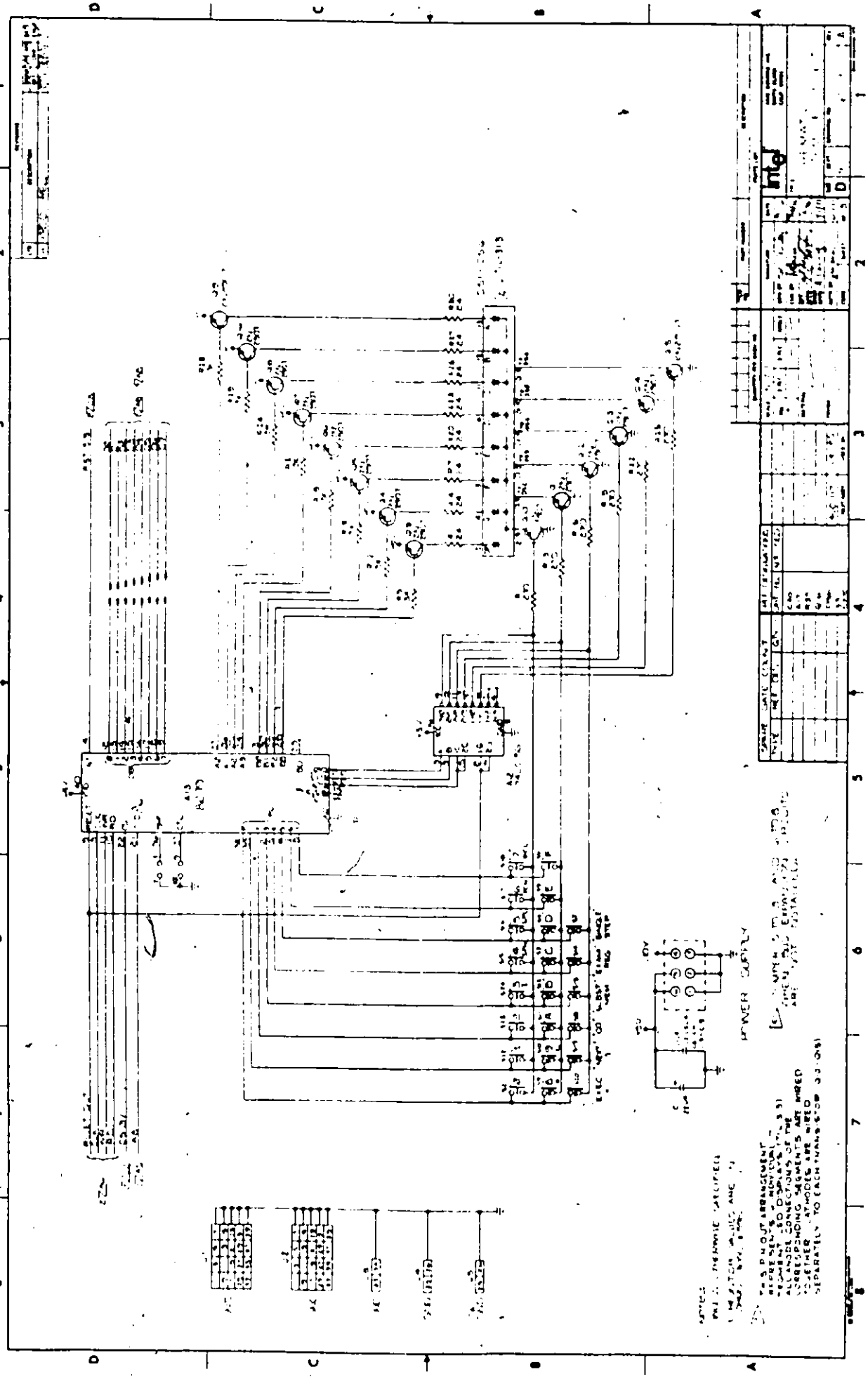

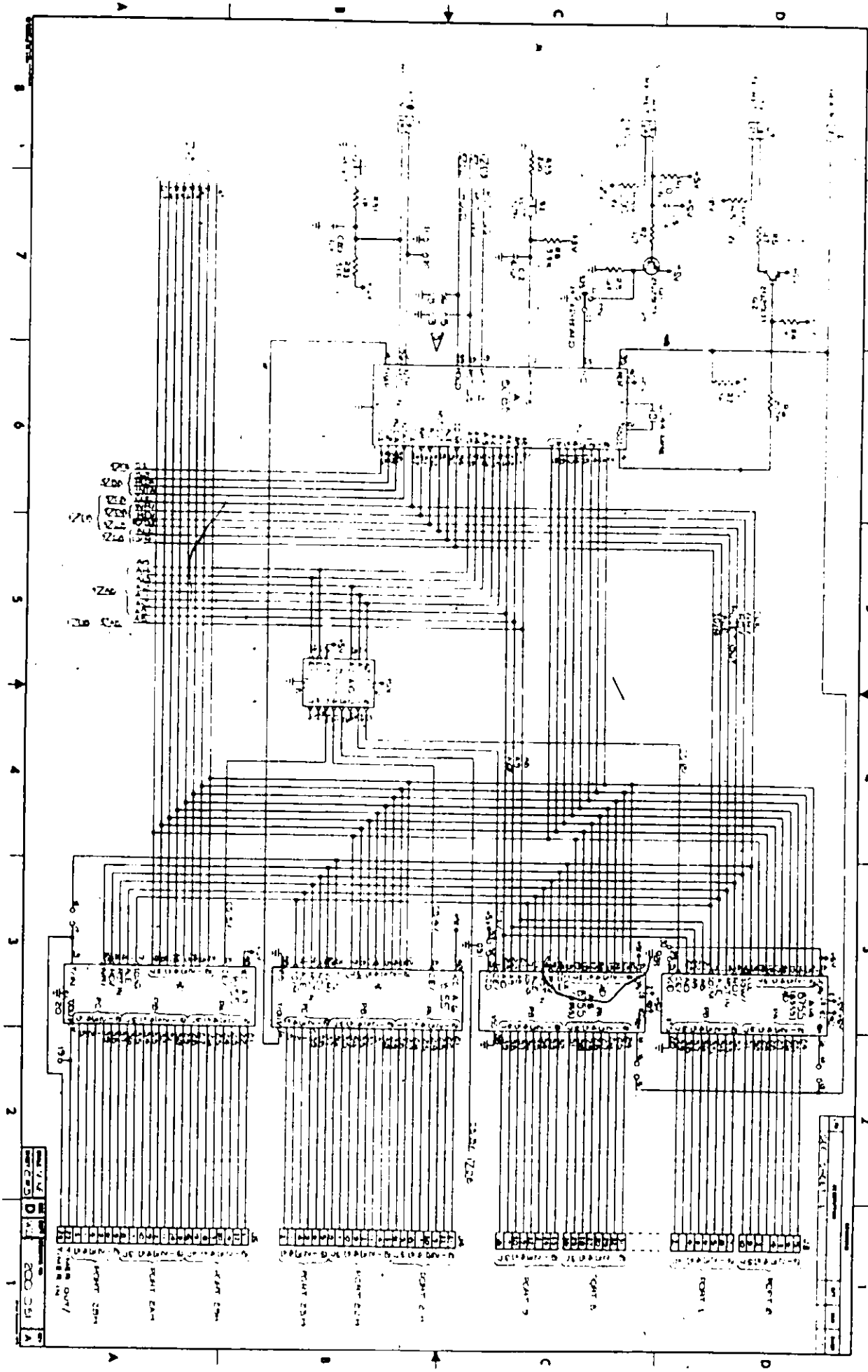

B.0 NOTES ON CSR SYSTEM SOFTWARE DESIGN

In this thesis the complete hardware design was specified. Appendix A contains all detailed circuit diagrams. Appendix C contains the data sheets of all hardware used for the CSR system. The CSR system software detailed design should follow the following guidelines.

B.1 DATA ACQUISITION MODULE

The CSR is designed to handle up to five input analog channels. Digital control of the AD501 analog multiplexer (MUX) is achieved through four bits of I/O port 23H of the master processor. The bit functions of port 23H are shown in figure B.1.

p3	p2	p1	p0	Analog channel selected
1	0	0	0	1
1	0	0	1	2
1	0	1	0	3
1	0	1	1	4
1	1	0	0	5
0	x	x	x	none

Figure B.1 Master processor I/O port 23H bit functions

The MUX address is generated by software, the number of input analog channels to sample being user selectable from 2 to 5.

The MUX address should be changed immediately after the A/D is read by the master processor.

Data acquisition is initiated when the start button is pressed (Figure A.1, D5). At this point the 8253 real time clock is enabled which in turn generates the proper negative pulses, through the 74123 monostable multivibrator, which initiates the A/D conversion on the AD574 analog converter (R/C signal). The AD574s "end of conversion" signal (STS signal) is used both for the hold signal on the AD582 sample and hold amplifier (SHA), and for interupting the master processor on RST6.5 when the A/D conversion cycle ends as indicated by a low going STS signal. At this point the master processor reads the 12 bits on the AD574 through 8 bits on I/O port 00H and 4 bits on I/O port 01H.

The RST6.5 interrupt handling routine on the master processor requires about 30 instructions for performing the following functions:

- A/D output buffer control
- read A/D 12 bits
- shared memory management

- analog multiplexer channel seletion

At an average 3.2 usec per instruction this requires about 100 usec. At the maximum CSR data acquisition rate of 1500 samples/secit leaves about 567 usec/sample to the processor for processing.

B.2 PROGRAMMABLE REAL TIME CLOCK

The 8253 programmable clock is used for generating the A/D sampling rate (through counter 0), and for the serial I/O timing for cassette recorder transfers (through counter 1) on the slave processor.

The reference clock signals used for both counters is derived from the 8085 processor clock signal which is divided by 2 through the 7473 JK flip-flop (i.e. reference rate of 1.5 MHz).

The real time clock output rates must therefore be determined by the master processor before data acquisition is initiated. This depends on the number of analog channels to be sampled and the sampling rate of each (note that the maximum aggregate rate of the CSR is 1500 samples per second).

For example if two channels are being sampled at 500 Hz each then

counter 0 count is 1.5 MHz / 0.001 MHz = 1500. Since the serial I/O rate to the cassette recorder is 24 KHz then counter 1 count is 1.5 MHz / 0.024 MHz = 63.

The real time clock counts are programed through the master processor I/O port 83H with the control word format shown in Figure B.2.

Port 83H control word	p7	p6	p5	p4	p3	p2	p1	p0
	sc1	sc0	rl1	rl0	m2	m1	m0	bcd

sc1	sc0	Function
0	0	select counter 0
0	1	select counter 1
1	0	select counter 2
1	1	illegal

rl1	rl0	Function
0	0	counter latching operation
0	1	read/load count less significant byte
1	0	read/load count most significant byte
1	1	illegal

m2	m1	m0	Function
1	1	1	set mode 3 (only mode used in CSR)
x	x	x	not used

bcd = 0 for binary 16 bit count

Figure B.2 Master processor I/O port 83H bit functions

B.3 BUS MULTIPLEXER

The master processor is responsible for assigning the two 2K RAM blocks to itself (for filling with input sampled data) or to the slave processor (for dumping output data to the cassette recorder). Refering to diagram A.2 (Bus Multiplexer) the two RAM blocks consist of pairs of 4118 static RAM chips; where B16 and B17 are assigned to block 1 and B18 and B19 to block 2. The master processor controls memory block-processor designation by setting the 8286 bidirectional bus drivers tri-state outputs through bits 0 and 1 of I/O port 21H as shown in Figure B.3.

Note that the transmit direction of B8, B9, B12 and B13 are always in the same B to A mode. The transmit direction of B10, B11, B14, B15 need to be controlled according to whether memory read or write is occuring. This is however controlled in hardware.

p2	p1	Block 1 designation	Block 2 designation
0	0	master	slave
0	0	slave	master

Figure B.3 Master processor I/O port 21H bit functions

B.4 CASSETTE DRIVE INTERFACE

The cassette drive subsystem control is the responsability of the slave processor under the direction of the master processor. The slave processor must perform the following tasks: tape rewinding to cassette load point from anywhere on the tape; fast forwarding; reading and writing blocks of data; padding write data with start, stop and parity bits and rmoving these bits from write data; and cassette track selection. This control is achieved through port 01H (for drive control signals) and port 02H (for drive status signals). The functions of these ports is shown in figures B.4, B.5 and B.6.

Bit no.	Drive signal	Function
p0	TMS	40 usec pulses (indicates tape holes)
p1	RDY	0 = tape ready
p2	FP	1 = write protected
p3	DATAGAP	0 = no data transmitted for 2 msec
p4	TACH	tach pulses (speed of motor)
p5	x	not used
p6	x	not used
p7	x	not used

Figure B.4 Slave processor I/O port 02H bit functions (input status signals from cassette drive)

Bit no.	Drive signal	Function
p0	ITR	0 = move tape 1 = stop tape
p1	FWD	0 = forward tape motion 1 = backward tape motion
p2	FST	0 = fast mode 1 = slow mode (read/write)
p3	WR	0 = activate write current
p4	PTUF	1 = disable phase encoding
p5	PDTR	1 = enable phase encoding
p6	TK0	0 = track 1 enabled 1 = track 2 enabled
p7	x	not used

Figure B.5 Slave processor I/O port 01H bit functions (output control signals from cassette drive)

p7	p6	p5	p4	p3	p2	p1	p0	
0	x	0	1	1	0	1	0	rewind tape
0	x	0	1	1	0	0	0	forward fast
0	x	1	0	0	1	0	0	write data
0	x	0	1	1	1	0	0	read data
0	x	0	1	1	0	0	1	stop tape

Figure B.6 Cassette drive control functions through slave processor I/O port 01H

B.5 PROCESSORS MEMORY MAPS

Figures B.7 and B.8 shows the memory maps for the master and slave processors respectively.

0000-07FF	SDK85 monitor ROM
1000-17FF	CSR program memory (2716 EPROM)
1800-1FFF	SDK85 keyboard/display controller area
2000-20FF	basic SDK85 RAM area
2800-28FF	CSR data memory (SDK85 expansion RAM)
3000-33FF	CSR buffer memory (block 1)
3800-3BFF	CSR buffer memory (block 2)

Figure B.7 Master processor memory map

0000-07FF	CSR program memory (2716 EPROM)
1000-13FF	CSR buffer memory (block 1)
2000-23FF	CSR buffer memory (block 2)

Figure B.8 Slave processor memory map